

AD-A016 772

COMPUTER SIMULATION OF RANDOM ATMOSPHERICALLY DEGRADED
OPTICAL BEAMS

S. A. Collins, Jr., et al

Ohio State University

Prepared for:

Rome Air Development Center
Defense Advanced Research Projects Agency

September 1975

DISTRIBUTED BY:

NTIS

National Technical Information Service
U. S. DEPARTMENT OF COMMERCE

315122

AD A016772

RADC-TR-75-222
Final Technical Report
September 1975



COMPUTER SIMULATION OF RANDOM ATMOSPHERICALLY
DEGRADED OPTICAL BEAMS

Ohio State University

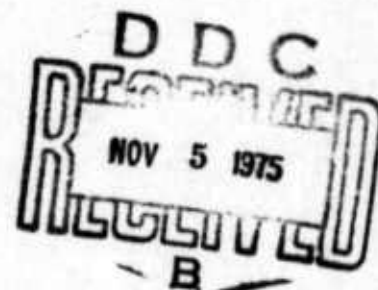
Sponsored by
Defense Advanced Research Projects Agency
ARPA Order No. 2646

Approved for public release;
distribution unlimited.

The views and conclusions contained in this document are those of the authors and should not be interpreted as necessarily representing the official policies, either expressed or implied, of the Defense Advanced Research Projects Agency or the U. S. Government.

Reproduced by
NATIONAL TECHNICAL
INFORMATION SERVICE
U.S. Department of Commerce
Springfield, VA 22151

Rome Air Development Center
Air Force Systems Command
Griffiss Air Force Base, New York 13441



This report has been reviewed by the RADC Information Office (OI) and is releasable to the National Technical Information Service (NTIS). At NTIS it will be releasable to the general public including foreign nations.

This report has been reviewed and is approved for publication.

APPROVED:

Darryl P. Greenwood

DARRYL P. GREENWOOD, Capt, USAF
Project Engineer

ACCESSION FOR	
DTIC	White Section <input type="checkbox"/>
DTIC	Blue Section <input type="checkbox"/>
DTIC	Red Section <input type="checkbox"/>
JUN 11 1964	
PV	
DISTRIBUTION AVAILABILITY CODES	
Dist.	PRICED, EXT. OR SPECIAL
A	

Do not return this copy. Retain or destroy.

COMPUTER SIMULATION OF RANDOM ATMOSPHERICALLY
DEGRADED OPTICAL BEAMS

S. A. Collins, Jr.
D. D. Duncan

Contractor: Ohio State University
Contract Number: F30602-74-C-0130
Effective Date of Contract: 24 January 1974
Contract Expiration Date: 14 January 1975
Amount of Contract: \$30,000.00
Program Code Number: 4E20
Period of work covered: 24 Jan 74 - 14 Jan 75
Principal Investigator: Dr. Stuart A. Collins, Jr.
Phone: 614 422-5045
Project Engineer: Capt Darryl P. Greenwood
Phone: 315 330-3145

Approved for public release;
distribution unlimited.

This research was supported by the Defense
Advanced Research Projects Agency of the
Department of Defense and was monitored by
Capt Darryl P. Greenwood, RADC (OCSE),
Griffiss Air Force Base, New York 13441.

UNCLASSIFIED

SECURITY CLASSIFICATION OF THIS PAGE (When Data Entered)

REPORT DOCUMENTATION PAGE		READ INSTRUCTIONS BEFORE COMPLETING FORM
1. REPORT NUMBER RADC-TR-75-222	2. GOVT ACCESSION NO.	3. RECIPIENT'S CATALOG NUMBER
4. TITLE (and Subtitle) COMPUTER SIMULATION OF RANDOM ATMOSPHERICALLY DEGRADED OPTICAL BEAMS		5. TYPE OF REPORT & PERIOD COVERED Final Technical Report 24 Jan 74 - 14 Jan 75
		6. PERFORMING ORG. REPORT NUMBER (3862-2)
7. AUTHOR(s) S. A. Collins, Jr. D. D. Duncan		8. CONTRACT OR GRANT NUMBER(s) F30602-74-C-0130
9. PERFORMING ORGANIZATION NAME AND ADDRESS Ohio State University Electro Science Laboratory 1320 Kinnear Rd, Columbus OH 43212		10. PROGRAM ELEMENT PROJECT TASK AREA & WORK UNIT NUMBERS 62301E 26460101
11. CONTROLLING OFFICE NAME AND ADDRESS Defense Advanced Research Projects Agency 1400 Wilson Blvd Arlington VA 22209		12. REPORT DATE September 1975
14. MONITORING AGENCY NAME & ADDRESS (if different from Controlling Office) Rome Air Development Center (OCSE) Griffiss AFB NY 13441		13. NUMBER OF PAGES 67
		15. SECURITY CLASS (of this report) UNCLASSIFIED
		15a. DECLASSIFICATION DOWNGRADING SCHEDULE N/A
16. DISTRIBUTION STATEMENT (of this Report) Approved for public release; distribution unlimited.		
17. DISTRIBUTION STATEMENT (of the abstract entered in Block 20, if different from Report) Same		
18. SUPPLEMENTARY NOTES RADC Project Engineer: Capt Darryl P. Greenwood/OCSE		
19. KEY WORDS (Continue on reverse side if necessary and identify by block number) Propagation Optical Atmospheric Simulation Computer		
20. ABSTRACT (Continue on reverse side if necessary and identify by block number) In this report there is developed a scheme for simulating randomly degraded optical beams including both phase and log-amplitude and the effect of their cross-correlation. The scheme works for optical degradations whose scale lengths range from much smaller to much larger than the input aperture size. An extension of the well-known Fourier transform method is used for the small scale fluctuations and a polynomial approach is used for the larger scale fluctuations. ia		

DD FORM 1 JAN 73 1473

EDITION OF 1 NOV 65 IS OBSOLETE

UNCLASSIFIED

SECURITY CLASSIFICATION OF THIS PAGE (When Data Entered)

CONTENTS

	Page
1. INTRODUCTION	1
2. GENERAL STATEMENT OF PROBLEM AND FREQUENCY DIVISION	2
3. HIGH SPATIAL FREQUENCY REPRESENTATION	8
4. LOW SPATIAL FREQUENCY REPRESENTATIONS	12
5. RESULTS	19
6. SUMMARY	43
7. CONCLUSIONS	45
APPENDIX A - SPECTRA	47
APPENDIX B	56
APPENDIX C	60
APPENDIX D	62
REFERENCES	63

This report deals with the digital simulation of optical wavefronts which have been degraded by propagation through a turbulent atmosphere. Such simulated wavefronts are necessary in the computer simulation of optical systems operating on atmospherically degraded light. Such system simulation is very desirable because of the expense of building prototype systems and testing them at remote locations after construction. The prime motivation is computer testing of compensated imaging systems for viewing objects at extremely large distances through the atmosphere.

The computer generated wavefronts to be described here are characterized by other factors. They simulate light which has propagated vertically through the atmosphere and have as a result an extremely long outer scale. The wavefronts also include amplitude as well as phase fluctuations and the effect of the cross correlation between them.

1. INTRODUCTION

In the past, two techniques have been used to generate members of random ensembles: the Fourier transform technique and the orthogonal polynomial technique. In the Fourier transform technique the power spectrum of the random function is assumed known. An array of uncorrelated gaussian random numbers with zero mean and unit variance is generated using standard digital computer programs. The Fourier transform of the array is computed and multiplied by the square root of the power spectrum and the inverse Fourier transform of the product is computed. The resulting array still has gaussian random variables but the correlation function is now that related to the power spectrum as desired.

In the orthogonal polynomial technique the random function is represented as a sum of orthogonal polynomials, with random coefficients. For example one might use Zernike polynomials to represent a random function in a round aperture. This scheme is fraught with peril however, unless the polynomials happen be statistically independent. Otherwise there will be cross-correlation between the various polynomial coefficients. A more desirable approach would use the Karhunen-Loève technique (Davenport, 1958) in which a set of polynomials is generated which are eigenfunctions of the covariance function. The random function is then expanded as a series of these eigenfunctions. Coefficients of the eigenfunctions are then known to be statistically independent.

Simulation of random atmospheric quantities has been performed using the Fourier transform technique (Hogge, 1973), (Bradley, 1974) where refractive index variations were generated. The Fourier transform technique has also been used (McGlamery, 1974), (Brown, 1974) for the simulation of respectively two and one dimensional random phase fronts.

Random wavefronts have also been generated using a sum of Zernike polynomials (Noll, 1974) and the Cholesky decomposition (Bradley, 1974). The work herein also related to the wavefront polynomial fitting scheme of Fried (1965) and to general work on Karhunen-Loève series.

In this report we extend previous work in that both log-amplitude as well as phase are considered as well as their cross-correlation. We also consider spatial spectra of much larger frequency range than heretofore used. The result is an approach which combines both the polynomial and Fourier transform technique approaches in an optimum fashion.

In this paper a random wavefront is represented as the sum of several terms, each pertaining to a different spatial frequency range. In each range a technique appropriate to the range is used to generate both phase and log-amplitude fronts. In the highest spatial frequency range the Fourier transform technique is used, extended to produce phase as well as log-amplitude fronts. In the lower spatial frequency ranges where the fluctuations are less rapid a polynomial scheme is used which starts out with a set of polynomials similar to Fried's but including more terms and ends up with the statistically independent Karhunen-Loève polynomials. These are then summed with random independent coefficients to provide a particular manifestation.

In the balance of the paper we will first present the physical picture considered along with a description of the spectral separation technique. Then the high frequency problem will be considered, including coupled phase and log-amplitude. In the next section the development of the polynomial fitting scheme used for the lower spatial frequency ranges will be presented. This will include the generation of a set of polynomials and their diagonalization to form the Karhunen-Loève functions. Following that the result of all the techniques is demonstrated and a typical representation shown. The final section contains discussion, summary and conclusions.

2. GENERAL STATEMENT OF PROBLEM AND FREQUENCY DIVISION

The general physical picture which we are considering is shown in Fig. 1 where we see a light beam propagating from a great height down through an atmosphere with fluctuating refractive index to the input aperture of an optical system. It is assumed that the outer scale L_0 and the structure parameter C_n of the turbulent fluctuations vary with height.

We desire to generate an ensemble of random phase and log-amplitude fronts over the input aperture. The phase and log-amplitude fronts should be normally distributed with the spatial autocovariances and crosscovariances or equivalently the spatial power spectra and cross spectra appropriate to the situation. Finally the phase and log-amplitude should respond faithfully to all scale sizes from the largest to the smallest.

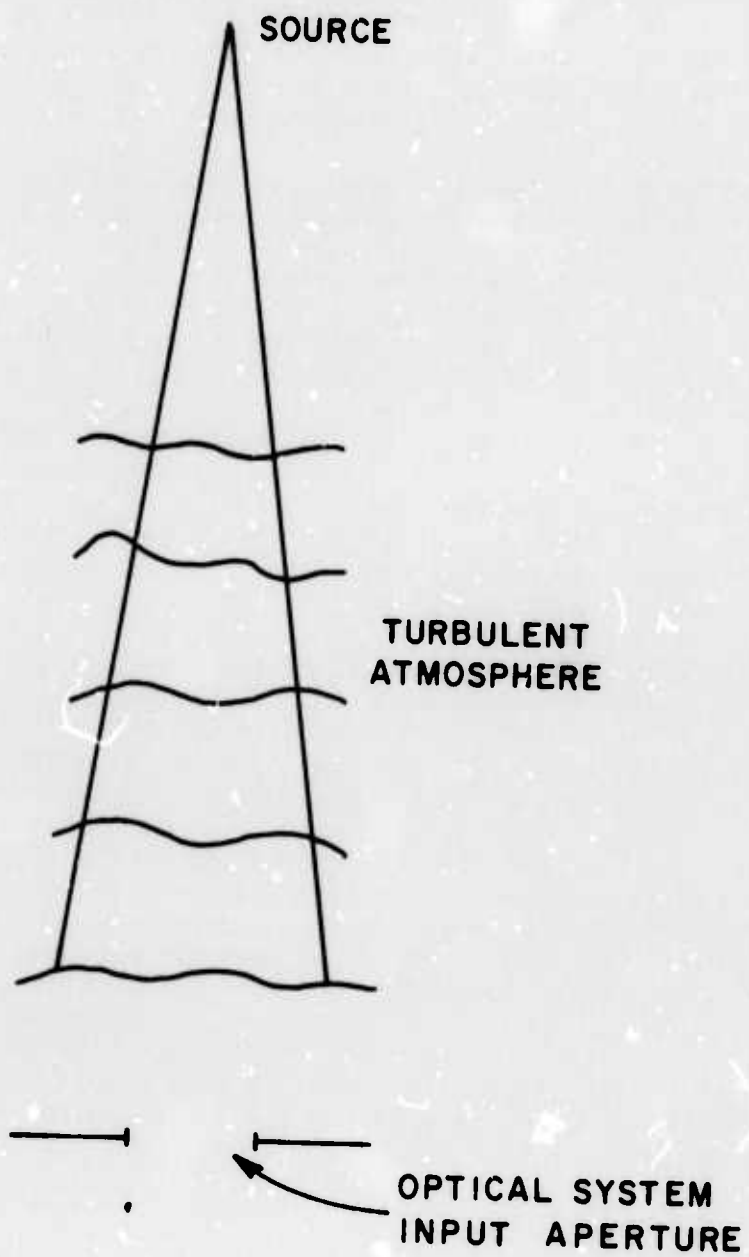


Fig. 1. Illustration of physical situation considered.

The spatial spectra of the phase and log-amplitude auto-covariances and their cross-covariance are calculated in Appendix A and are shown graphically in Fig. 2 for a coherence length r_0 of 60 cm wavelength of 0.6328 microns and ratio of source height to receiver height of 10^4 . They were calculated using standard techniques (Tatarski, 1971).

Examination of the spectra reveal one major problem, the tremendous strength associated with the low spatial frequencies corresponding to scale sizes much larger than the aperture. We note that the knee in the phase spatial spectrum curve occurs at $\kappa = 10^{-5} \text{ rad} \cdot \text{m}^{-1}$ which corresponds to a spatial scale of 6×10^5 meters. If we were going to use the Fourier transform technique without any modifications we would need a grid at least 10^5 meters on a side and with elements much smaller than the input aperture, say a millimeter in size. That indicates a square matrix array with 10^8 elements on a side, indeed not the simplest task. If a coarser grid were used there would be too rapid a change between the lowest spatial frequency component and the next higher one. With such a rapid change in the spectrum the discrete Fourier transform operation would not faithfully represent the spatial behavior without aliasing.

Another part of the problem is that the large scale fluctuations are much larger than the aperture size. The large scale fluctuations will have relatively smooth variations over the size of the aperture. Some method must be found for representing only the portion of the large scale fluctuations which are present.

In order to solve the problem of representing the large scale fluctuations we conceptually split the representation problem into two parts: dividing the spatial spectrum and relating the portions of the spatial spectrum to fields over the aperture. We first consider the problem of dividing the spatial spectrum into sections.

To continue we split the spatial spectrum up into regions, each region being sufficiently small so that it can be represented by a reasonable number of discrete points. Thus the two-dimensional spatial spectrum would be

$$(1) \quad F(\vec{\kappa}) = \sum_0^4 F_n(\vec{\kappa})$$

where F_0 is the contribution to the spatial spectrum from the highest spatial frequency range, F_1 is the contribution from the next to highest frequency range and so on. The various spectral ranges are centered about the origin and have the following frequency limits.

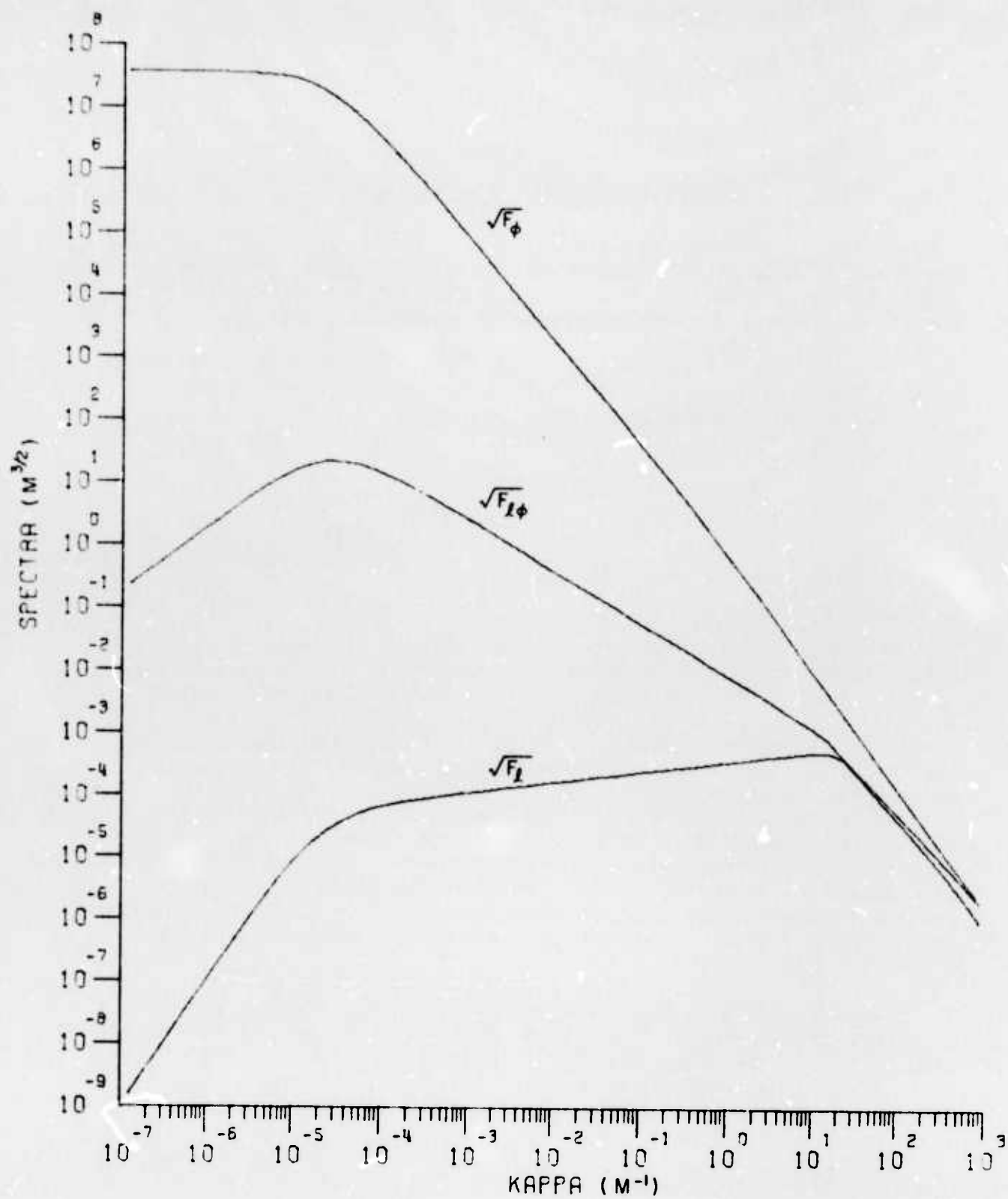


Fig. 2. Log-log plots of square root of spectra of log-amplitude and phase covariances and of phase-log-amplitude cross covariance.

$$\begin{array}{ll}
n = 0 & -32 \times 2\pi \leq \kappa_x, \kappa_y \leq 31 \times 2\pi \\
n = 1 & -2\pi \leq \kappa_x, \kappa_y \leq (31/32)2\pi \\
n = 2 & -2\pi/32 \leq \kappa_x, \kappa_y \leq (31/32)2\pi/32 \\
n = 3 & -2\pi/32^2 \leq \kappa_x, \kappa_y \leq (31/32)2\pi/32^2 \\
n = 4 & -2\pi/32^3 \leq \kappa_x, \kappa_y \leq (31/32)2\pi/32^3
\end{array}$$

The fraction 31/32 occurs because the element (33,33) was chosen to represent the zero spatial frequency. Thus each spectral region corresponds to a square spatial region 32^n meters on a side.

In the discrete representation used for the spectrum in the highest spatial frequency range all but the zero frequency spectral value are identical to the true spectral value

$$(2) \quad F_0(\kappa_x, \kappa_y) = F(\kappa_x, \kappa_y) \left\{ \begin{array}{l} \kappa_x = 2\pi(k-33) \\ \kappa_y = 2\pi(33-L) \\ \kappa_x, \kappa_y \neq 0 \end{array} \right\} 1 < K, L < 64$$

The value at zero frequency is somewhat arbitrarily chosen. This is necessary because the actual value for some of the spectra is vastly different from that of the first harmonic, so that aliasing would result in the corresponding position function if it were used. To avoid this a particular procedure is used. We impose the requirement that a finite Fourier series representation of the spectrum represent the spectrum not only at the discrete points but in between the points also. To check this requirement a value of the spectrum at zero frequency is chosen approximately equal to the value at the first harmonic. The spectrum is represented as a finite Fourier series and then evaluated at non-integral values of K and L. For a reasonable value of the zero frequency component the spectrum varies smoothly from one point to another. For an improper choice there are oscillations or ringing between the discrete points.

For the next, $n=1$, region of the spatial spectrum a discrete representation is also used. In this case it will be used as an intermediate step. The discrete representation is formed from the true spectrum with the spectrum for $n=0$ subtracted. In essence this means that the spectrum for $n=0$ is evaluated at each of the discrete points between zero and the first harmonic

$$(3) \quad \begin{aligned} \kappa_x &= 2\pi(K-33)/32 \\ \omega_y &= 2\pi(33-L)/32 \end{aligned} \quad 1 \leq K, L \leq 64$$

and subtracted from the true spectrum at those points. This procedure has the advantage that the newly formed spectrum goes to zero at the edge of the spectral region thus rendering it automatically band-limited. The zero frequency spectral value in the $n=1$ region is determined in a manner identical to that used in region $n=0$.

The procedure for the other spectral regions is identical to that used in region $n=1$.

The procedure for generating random arrays over the one meter aperture from the spectra associated with all but the highest spatial frequency spectral region involves a procedure using polynomials. This will be described presently. First to form the basis we consider a simpler approach.

With the spectra decomposed as indicated it is a simple matter to use the Fourier transform procedure to generate five sets of random arrays of different sizes and to find the contribution to an area one meter square in the center of the larger arrays. One would need some sort of interpolation procedure to go from the discrete arrays to a much smaller grid a meter square. Then the sum of all the contributions over the square meter would represent the wavefront. This would be the direct approach.

We use an alternative and operationally faster procedure for finding the contributions over the square meter aperture arising from the lower spectral ranges. The procedure as indicated previously is to expand the contribution to the phase front across the aperture in a series of polynomials with random coefficients. The variances of the coefficients are determined from the spectra for the given range.

One might envision the procedure as having the following steps. Suppose we were to use the Fourier transform procedure to calculate a large number of random wavefronts for each of the spectral regions. The wavefront contribution corresponding to the highest frequency spectral range is retained for use as is. Then suppose we choose a one meter square with 64^2 points in the center of all random wavefronts for each of the other spectral ranges. We then interpolate from the large square grids to the one meter square grid. The interpolation should be performed assuming that the Fourier series representation for each random manifestation was a continuous one and evaluating it at the 64^2 points in the central one meter array. Alternatively the sampling theorem could be used for the interpolation. The values at the 64^2 points for each manifestation would be used to find the coefficients for a polynomial expansion of the manifestation. The coefficients would vary randomly from

one manifestation to another. Indeed since the wavefronts vary randomly with normal distribution and zero mean the polynomial coefficients will also vary randomly with zero mean. One would find the variance of the coefficients for each spectral range by averaging the square of each coefficient over the set of manifestations.

Thus one would end up with a polynomial series for each spectral range representing the front over the central square meter. The coefficients of the polynomials would be normally distributed with zero mean and known variances. To generate another random manifestation one would merely generate a new set of coefficients using standard random number generation schemes. Assuming the number of random coefficients required is less than 642 the procedure is quicker.

In the procedure to follow one further step will be added, slightly complicating the mathematics. That is that polynomials will be found that will simultaneously represent both phase and log-amplitude. Also the Fourier transform procedure that is used directly for the highest spatial frequency portion of the spectrum must be modified to simultaneously generate both phase and log-amplitude fronts.

In the next section the extension of the basic Fourier transform procedure to include coupled phase and log-amplitude will be considered. In the section to follow the polynomial approach used for the lower regions of the spatial spectrum will be derived in general terms.

3. HIGH SPATIAL FREQUENCY REPRESENTATION

We now describe the procedure used to generate the contribution to the random wavefronts from the highest spatial frequency region. The procedure used is based on the Fourier transform approach but is more general. The approach is extended to two random fronts, phase and log-amplitude, which are correlated. The basic expressions derived here will also be used in the next section in the derivation of the representation for the lower spatial frequency contributions. We assume that the spectra of the phase and log-amplitude covariance functions $F_\phi(\kappa_x, \kappa_y)$ and $F_\ell(\kappa_x, \kappa_y)$ respectively, as well as the spectrum of their cross-covariance, $F_{\ell\phi}(\kappa_x, \kappa_y)$ are available.

The procedure will be to postulate a particular model and then show that it can be made to have the desired properties. To begin, for a single manifestation we generate two square matrices, $R_1(I, J)$ and $R_2(I, J)$ of statistically independent samples (Hogge, 1974) from a distribution which is gaussian with zero mean and unit variance. Stated mathematically, this is

$$(4) \quad \langle R_i(I, J) R_j(K, L) \rangle = \delta_{i,j} \delta_{I,K} \delta_{J,L}$$

where the angular brackets denote the expectation operator. We then postulate that the discrete spectra of the phase and log-amplitude covariances can be represented respectively by

$$(5a) \quad \phi(K_{\kappa_0}, L_{\kappa_0}) = F_a(K_{\kappa_0}, L_{\kappa_0})R_1(K, L) + F_b(K_{\kappa_0}, L_{\kappa_0})R_2(K, L)$$

$$(5b) \quad \mathcal{L}(K_{\kappa_0}, L_{\kappa_0}) = F_a(K_{\kappa_0}, L_{\kappa_0})R_1(K, L) + F_b(K_{\kappa_0}, L_{\kappa_0})R_2(K, L) \quad .$$

In Eqs. (5) K and L are integers, κ_0 is the numerical value of the spatial frequency spacing, and the spectra F_a , F_b , F_c are as yet undefined. The values of κ_0 will depend upon the particular spatial frequency range.

The desired expected values are

$$(6a) \quad \langle \phi(K_{\kappa_0}, L_{\kappa_0}) \rangle = \langle \mathcal{L}(K_{\kappa_0}, L_{\kappa_0}) \rangle = 0$$

$$(6b) \quad \langle |\phi(K_{\kappa_0}, L_{\kappa_0})|^2 \rangle = \kappa_0^{-2} F_{\phi}(K_{\kappa_0}, L_{\kappa_0})$$

$$(6c) \quad \langle \mathcal{L}(K_{\kappa_0}, L_{\kappa_0}) \phi^*(K_{\kappa_0}, L_{\kappa_0}) \rangle = \kappa_0^{-2} F_{\phi\mathcal{L}}(K_{\kappa_0}, L_{\kappa_0})$$

$$(6d) \quad \langle |\mathcal{L}(K_{\kappa_0}, L_{\kappa_0})|^2 \rangle = \kappa_0^{-2} F_{\mathcal{L}}(K_{\kappa_0}, L_{\kappa_0}) \quad .$$

To evaluate the unknown functions F_a , F_b , and F_c we substitute Eqs. (5) into Eqs. (6) to obtain

$$(7a) \quad \kappa_0^{-2} F_{\phi} = \langle |\phi|^2 \rangle = |F_a|^2 \langle |R_1|^2 \rangle + |F_b|^2 \langle |R_2|^2 \rangle = |F_a|^2 + |F_b|^2$$

$$(7b) \quad \kappa_0^{-2} F_{\phi\mathcal{L}} = \langle \phi \mathcal{L}^* \rangle = F_a F_c^* \langle |R_1|^2 \rangle + |F_b|^2 \langle |R_2|^2 \rangle = F_a F_c^* + |F_b|^2$$

$$(7c) \quad \kappa_0^{-2} F_{\mathcal{L}} = \langle |\mathcal{L}|^2 \rangle = |F_c|^2 \langle |R_1|^2 \rangle + |F_b|^2 \langle |R_2|^2 \rangle = |F_c|^2 + |F_b|^2.$$

In Eqs. (7), use has been made of the statistical independence of the matrix elements stated in Eq. (4). Solving Eqs. (7) for F_a , F_b , and F_c , we obtain (for the case where F_a , F_b and F_c are real),

$$(8a) \quad F_a = \frac{F_\phi - F_{\ell\phi}}{\kappa_0 \sqrt{F_\phi - 2F_{\ell\phi} + F_\ell}}$$

$$(8b) \quad F_b = \frac{\sqrt{F_\phi F_\ell - F_{\ell\phi}^2}}{\kappa_0 \sqrt{F_\phi - 2F_{\ell\phi} + F_\ell}}$$

$$(8c) \quad F_c = \frac{F_\phi - F_\ell}{\kappa_0 \sqrt{F_\phi - 2F_{\ell\phi} + F_\ell}}$$

These three spectra are displayed in Fig. 3 for the complete spectrum. Note that the magnitude of F_c is plotted since it becomes negative at $\kappa \approx 10\pi$.

Thus to generate one sample wavefront the procedure is to generate the two random matrices, $R_1(K,L)$ and $R_2(K,L)$ and then $\phi(K\kappa_0, L\kappa_0)$ and $\chi(K\kappa_0, L\kappa_0)$ using Eqs. (5) and then to take the inverse transform using

$$(9a) \quad \phi(Ix_0, Jx_0) = \kappa_0^2 \iint \phi(K\kappa_0, L\kappa_0) e^{\frac{-j2\pi[(I-1)(K-1) + (J-1)(L-1)]}{N_0}}$$

$$(9b) \quad \chi(Ix_0, Jx_0) = \kappa_0^2 \iint \chi(K\kappa_0, L\kappa_0) e^{\frac{-j2\pi[(I-1)(K-1) - (J-1)(L-1)]}{N_0}}$$

Equations (5) and (8) completely describe the desired model for the generation of random wavefronts. The model requires the use of two arrays of random numbers, and three spectra which are nonlinear combinations of phase and log-amplitude and cross covariance power spectra. Wavefronts generated by this model have been demonstrated to have the correct first and second order statistics.

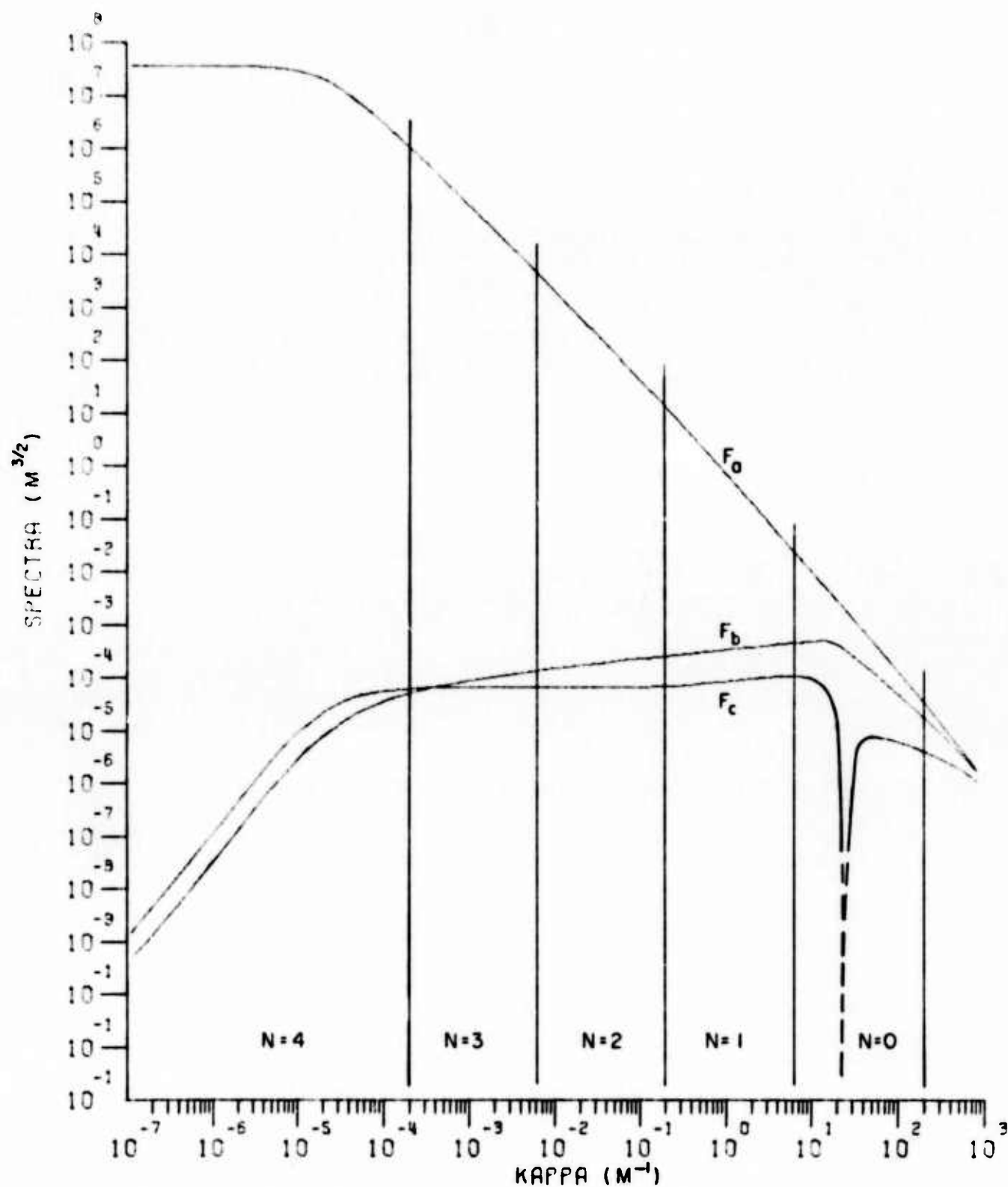


Fig. 3. Log-log plots of square root of spectra F_a , F_b , and F_c . The absolute value of F_c is plotted since F_c becomes negative around $\kappa \pm 2\pi$.

For the case at hand where the spectra must be divided into regions it is the spectra F_a , F_b , and F_c which would be divided since it is those spectra from which the random spectra and random wavefronts are generated. Thus the procedure would be to take the spectra in Fig. 3 which have been formed from the undivided log-amplitude, phase and cross spectra of Fig. 2 and apply the spectral divisions, and find the best zero frequency value. Equations (3) (8) and (9) then give the wavefront manifestations, applicable to any spectral region.

In this section we have considered the generalization of the Fourier transform procedure to the case of coupled phase and log-amplitude. The equations for generation of the combined random fronts have been derived. The procedure is applicable to all spectral regions, although it will be used for only the highest frequency region. The procedure will be combined with the polynomial approach for use in the lower spatial frequency regions in the next section.

4. LOW SPATIAL FREQUENCY REPRESENTATIONS

In this section we consider in detail the representation for the lower frequency regions of the spatial spectrum. The development is based on a polynomial representation and applies to both phase and log-amplitude and their cross correlation.

In the following both the phase and log-amplitude will have polynomial representations. That is, each manifestation of both the phase and log-amplitude will be represented over the input aperture by the polynomial series

$$(10a) \quad \phi(\vec{r}) = \sum_n \phi_n \phi_n(\vec{r})$$

$$(10b) \quad \psi(\vec{r}) = \sum_n \psi_n \phi_n(\vec{r})$$

where the $\phi_n(\vec{r})$ are a finite set of orthonormal polynomials defined over the input aperture and the coefficients ϕ_n , ψ_n are gaussian random variables with zero mean and variance yet to be determined. The various random coefficients are in general correlated, cross-correlations occurring both among the various log-amplitude coefficients and among the various phase coefficients and also occurring between log-amplitude and phase coefficients. The specific form of the individual polynomials for one situation will be shown in the next section. Using Eqs. (10) the contribution from the lower spatial frequency ranges then has the form

$$(11a) \quad \psi_1(\vec{r}) = \sum_{n=1}^N \epsilon_n \psi_n(\vec{r}) + j \sum_{n=1}^N \phi_n \psi_n(\vec{r}).$$

Our goal is to find another representation in terms of a new set of orthonormal polynomials $\epsilon_i(\vec{r})$ whose coefficients are also gaussian random variables with zero mean but whose coefficients are uncorrelated. The complex log-amplitude will then be expanded in a series of the new polynomials

$$(11b) \quad \epsilon_1(\vec{r}) = \sum c_i \epsilon_i(\vec{r})$$

This new polynomial series will then be used for the random wave-front generation. One merely generates the random coefficients, c_n , and sums the series at the desired values of r . The series with uncorrelated coefficients is desirable because standard computer-based random number generation schemes generally produce only uncorrelated random numbers.

The procedure for generating the polynomials whose coefficients will be uncorrelated is to diagonalize the covariance matrix of the multivariate gaussian distribution associated with the orthonormal polynomials. If there are N polynomials in the set, then there will be $2N$ gaussian random variables. N are for the coefficients of the log-amplitude representation and N are for the phase. Thus the joint probability density for the $2N$ random variables is (Davenport, 1958)

$$(12) \quad P(\phi_1, \dots, \phi_n, \epsilon_1, \dots, \epsilon_n) = (2\pi)^{-N} |Q| \exp - \frac{1}{2} \sum \sum Q_{\phi_n \phi_m} \phi_n \phi_m + \sum \sum Q_{\epsilon_n \epsilon_m} \epsilon_n \epsilon_m + \sum \sum Q_{\phi_n \epsilon_m} \phi_n \epsilon_m$$

where the matrix $\bar{Q} = \bar{C}^{-1}$ is the inverse of the covariance matrix, \bar{C} , including phase autocovariances, log-amplitude autocovariances, and phase-log-amplitude cross-covariances. The covariance matrix is defined by

$$(13a) \quad C_{\phi_n \phi_m} = \langle \phi_n \phi_m \rangle$$

$$(13b) \quad C_{\epsilon_n \epsilon_m} = \langle \epsilon_n \epsilon_m \rangle$$

$$(13c) \quad C_{n\phi m} = \langle \phi_n \phi_m \rangle$$

The calculation of the covariance matrix elements will be discussed later in this section.

The procedure for finding the new random independent coefficients is well known: transform to a new linear combination of coefficients which diagonalizes the quadratic form in the exponent of the joint probability density function. To illustrate this we use a matrix notation. The quadratic form, Q , in the exponent of Eq. (12) is written in vector notation

$$(14a) \quad 2Q = \bar{v}^T \bar{Q} \bar{v}$$

where the vector, v , is

$$(14b) \quad \bar{v} = (\phi_1, \phi_2, \dots, \phi_N, \phi_1, \phi_2, \dots, \phi_N)$$

and the matrix \bar{Q} is the inverse of the covariance matrix as indicated. To diagonalize the quadratic form find vectors, \bar{w} , satisfying the matrix eigenvalue equation

$$(15) \quad \bar{Q} \bar{w}_n = \lambda_n \bar{w}_n$$

Then the diagonalizing transformation is the modal matrix, \bar{M} , whose columns are the orthonormal eigenvectors, \bar{w}_n .

$$(16) \quad \bar{M}^T \bar{Q} \bar{M} = \bar{\Lambda}$$

$\bar{\Lambda}$ is the diagonal matrix containing the eigenvalues. Then the new random coefficients c_n are given by

$$(17) \quad \bar{v} = \bar{M} \bar{c}$$

where

$$(18) \quad c = (c_1, \dots, c_{2N}).$$

The c_n are the desired random independent variables. They are gaussian with zero mean because the ϕ_n and ψ_n are gaussian with zero mean. The c_n also have variances λ_{nn}^{-1} given by the diagonalized inverse covariance matrix.

The complex log-amplitude in Eq. (11) can be rewritten in terms of the new coefficients. Writing Eq. (11) in terms of a function vector,

$$(19) \quad \bar{\psi}(\bar{r}) = (\psi_1, \psi_2, \dots, \psi_N, j\psi_1, j\psi_2, \dots, j\psi_N)$$

we have

$$(20) \quad \phi_1(\bar{r}) = \bar{\psi}^T(\bar{r}) \bar{v}$$

$$(21) \quad = \bar{\psi}^T(\bar{r}) \bar{M} \bar{c}$$

$$(22) \quad = \bar{\xi}^T(\bar{r}) c = \sum c_n \xi_n(\bar{r})$$

where

$$(23) \quad \xi(\bar{r}) = (\xi_1(\bar{r}), \xi_2(\bar{r}), \dots, \xi_{2N}(\bar{r})) \equiv \bar{M}^T \bar{\psi}$$

Equation (22) is the desired result. The first order complex log-amplitude, ϕ_1 , is represented as a sum of orthonormal polynomials, the $\xi_n(\bar{r})$, with random uncorrelated coefficients, the c_n .

We note some interesting features in this solution. The polynomials $\xi_n(\bar{r})$ are in general complex, since the diagonalizing transformation mixes log-amplitude and phase. The solution is also identical to a solution of the Karhunen-Loève problem. This is demonstrated in Appendix B.

We now proceed to derive a general expression for the covariance matrix \bar{C} from which its inverse $\bar{Q} = \bar{C}^{-1}$ can be obtained. The derivation involves a several step procedure. Basically the steps amount to conceptually generating a wavefront which covers a large region using the Fourier transform technique. The statistical properties of this large wavefront are thus known from the proceeding section. Next imagine that we generate an ensemble of wavefronts and interpolate between the matrix of points using the sampling theorem representation. Imagine that we then take the center one square meter of each ensemble member and expand that in terms of the polynomial representation of Eqs. (10). We can then determine each of the ϕ_n and ψ_n for each ensemble member and further can determine the covariances $\langle \phi_m \phi_n \rangle$, $\langle \psi_m \psi_n \rangle$ and cross covariances, $\langle \phi_n \psi_m \rangle$ constituting the elements of the covariance matrix. In Eqs. (10) $\phi(\bar{r})$ and $\psi(\bar{r})$ are defined over a one square meter aperture. Using the orthonormality assumed for the polynomials $\psi_n(\bar{r})$ we can write

$$(24) \quad \phi_n = \iint \phi(\bar{r}) \psi_n(\bar{r}) w(\bar{r}) d\bar{r}$$

where $w(\bar{r})$ is the aperture function,

$$(25) \quad w(\bar{r}) = \begin{cases} 1 & \begin{cases} -1/2 \leq x \leq 1/2 \\ -1/2 \leq y \leq 1/2 \end{cases} \\ 0 & \text{otherwise} \end{cases}$$

The derivation of expressions for ϕ_n and ψ_n contains several steps. First we use the procedure of the proceeding section to produce a phase front at a large array of points by generating the random spectral matrices R_1 and R_2 and then the spectra $\phi(K_{x_0}, L_{x_0})$ and $\psi(K_{y_0}, L_{y_0})$ as indicated in Eqs. (7). We then take the inverse transform to obtain the phase over the large array.

$$(26) \quad \phi(Mx_0, Nx_0) = \kappa_0^2 \sum \sum \phi(K_{x_0}, L_{x_0}) e^{\frac{j2\pi}{N} ((K-1)(M-1) + (L-1)(N-1))}$$

We then assume that the spectra are band limited and write a sampling theorem expression for the phase at any point (x, y) .

$$(27) \quad \phi(x,y) = \sum_M \sum_N \phi(Mx_0, Nx_0) \text{sinc} \pi \left[\frac{x}{x_0} - (M-33) \right] \text{sinc} \pi \left[\frac{y}{x_0} - (33-N) \right]$$

where $\text{sinc}(u) \equiv \sin(u)/u$. Combining Eqs. (5), (24), (26) and (27) gives

$$(28) \quad \phi_M = \sum_{K,L} [F_a(K_{\kappa_0}, L_{\kappa_0}) R_1(K_{\kappa_0}, L_{\kappa_0}) + F_b(k_{\kappa_0}, L_{\kappa_0}) R_2(K_{\kappa_0}, L_{\kappa_0})] U_n(K_{\kappa_0}, L_{\kappa_0})$$

where

$$(29a) \quad U_n(K_{\kappa_0}, L_{\kappa_0}) = \kappa_0^2 \sum_M \sum_N V_n(Mx_0, Nx_0) e^{j \frac{2\pi}{N} ((K-1)(M-1) + (L-1)(N-1))}$$

and

$$(29b) \quad V_n(Mx_0, Nx_0) = \iint d\vec{r} w(r) \psi_n(\vec{r}) \text{sinc} \pi \left[\frac{x}{x_0} - (M-33) \right] \text{sinc} \pi \left[\frac{y}{x_0} - (33-N) \right]$$

A similar expression can be derived for the log-amplitude coefficients.

$$(29c) \quad \phi_n = \sum_K \sum_L [F_c(K_{\kappa_0}, L_{\kappa_0}) R_1(K_{\kappa_0}, L_{\kappa_0}) + F_b(K_{\kappa_0}, L_{\kappa_0}) R_2(K_{\kappa_0}, L_{\kappa_0})] U_n(K_{\kappa_0}, L_{\kappa_0}).$$

The covariance matrix elements then follow from Eqs. (13), (28), and (29).

$$(30a) \quad C_{\phi_n \phi_n} = \langle \phi_n \phi_n^* \rangle = \sum_K \sum_L \{ |F_a(K_{\kappa_0}, L_{\kappa_0})|^2 + |F_b(K_{\kappa_0}, L_{\kappa_0})|^2 \} U_m^*(k_{\kappa_0}, L_{\kappa_0}) U_n(K_{\kappa_0}, L_{\kappa_0})$$

$$= \sum_K \sum_L \kappa_0^{-2} F(K_{\kappa_0}, L_{\kappa_0}) U_m^*(K_{\kappa_0}, L_{\kappa_0}) U_n(K_{\kappa_0}, L_{\kappa_0})$$

$$\begin{aligned}
(30b) \quad C_{\ell_n \ell_m} = \langle \ell_n \ell_m^* \rangle &= \sum_K \sum_L \{ |F_c(K\kappa_0, L\kappa_0)|^2 + |F_b(K\kappa_0, L\kappa_0)|^2 \\
&\quad U_m^*(K\kappa_0, L\kappa_0) U_n(K\kappa_0, L\kappa_0) \\
&= \sum_K \sum_L \kappa_0^{-2} F_\ell(K\kappa_0, L\kappa_0) U_m^*(K\kappa_0, L\kappa_0) U_n(K\kappa_0, L\kappa_0)
\end{aligned}$$

$$\begin{aligned}
(30c) \quad C_{\ell_n \phi_m} = \langle \ell_n \ell_m^* \rangle &= \\
&= \sum_K \sum_L \{ F_a(K\kappa_0, L\kappa_0) F_c^*(K\kappa_0, L\kappa_0) + |F_b(K\kappa_0, L\kappa_0)|^2 \} \\
&\quad U_m^*(K\kappa_0, L\kappa_0) U_n(K\kappa_0, L\kappa_0) \\
&= \sum_K \sum_L \kappa_0^{-2} F_\ell(K\kappa_0, L\kappa_0) U_m^*(K\kappa_0, L\kappa_0) U_n(K\kappa_0, L\kappa_0)
\end{aligned}$$

Equations (35) together with Eqs. (33) constitute the formal solution for the covariance matrix. In the next section a particular set of polynomials will be chosen. To go with these the particular associated $V_n(Mx_0, Nx_0)$ and $U_n(K\kappa_0, L\kappa_0)$ are evaluated in Appendix C.

To summarize, we have considered in formal terms a method for generating the contribution to the random wavefront from the lower spatial frequency portions of the spectrum. A polynomial representation is derived in which the complex log-amplitude is expressed in terms of a series of complex orthonormal polynomials with random uncorrelated coefficients. The variances of the coefficients are related to the covariance matrix defined in terms of the cross correlation between the random expansion coefficients. General expressions for the covariance matrix elements are derived.

5. RESULTS

We now proceed to give the specific details for the random wavefront simulation. First the spectrum is partitioned and the low frequency problem is treated. Then after choosing a group of ten polynomials orthonormal over a source aperture of unit width, the resulting covariance matrices, eigenvectors and eigenvalues are listed. The high frequency problem which has been discussed previously is mentioned only in regards to the superposition of the two results. Finally a typical ensemble member, a single wave-front manifestation, is displayed.

The polynomials employed in the expansion of the wavefront are listed in Eqs. (31)

Group I

$$(31a) \quad \psi_0(x,y) = 1$$

$$(31b) \quad \psi_3(x,y) = 6\sqrt{\frac{5}{2}} \left(x^2 + y^2 - \frac{1}{6} \right)$$

$$(31c) \quad \psi_4(x,y) = 6\sqrt{\frac{5}{2}} (x^2 - y^2)$$

Group II

$$(31d) \quad \psi_5(x,y) = 12 xy$$

Group III

$$(31e) \quad \psi_1(x,y) = 2\sqrt{3} x$$

$$(31f) \quad \psi_6(x,y) = 12\sqrt{15} \left(xy^2 - \frac{1}{12} x \right)$$

$$(31g) \quad \psi_8(x,y) = 20\sqrt{7} \left(x^3 - \frac{3}{20} x \right)$$

Group IV

$$(31h) \quad \psi_2(x,y) = 2\sqrt{3} y$$

$$(31i) \quad \psi_7(x,y) = 12\sqrt{15} (yx^2 - \frac{1}{12} y)$$

$$(31j) \quad \psi_9(x,y) = 20\sqrt{7} (y^3 - \frac{3}{20} y)$$

As indicated the polynomials are chosen to be orthonormal over a unit square as described by Eq. (25).

The grouping of the polynomials in Eqs. (31) was done to indicate the similarities in symmetry. The first set $\psi_0(\vec{r})$, $\psi_2(\vec{r})$ and $\psi_4(\vec{r})$ employ the same combinations used by Fried (1965). They are even in both x and y. The second set, $\psi_5(\vec{r})$ is odd in both x and y. The third set is odd in x and even in y. The polynomials in the fourth set are identical with those in the third set except for a ninety degree rotation. As one might expect the statistical properties of the last two sets will be identical because the correlation functions and power spectra have central symmetry.

The next step after the choice of polynomials is the partitioning of the spectra. We used a trial and error procedure to choose new zero-frequency values for F_a , F_b , and F_c in the highest spatial frequency region. For F_a the zero frequency value chosen was 1.75 times the value for the first harmonic. For F_b and F_c the zero-frequency values were set equal to the values of the respective first harmonics. Plots of the difference spectra used for regions 1 and 2 are shown in Figs. 4. The circles indicate the values at the discrete points while the solid curve comes from the interpolated values. The last curve is an example of a poorly chosen zero frequency value.

The next step is the generation of the covariance matrix. There is a simplification that arises in the covariance matrix because of the symmetry properties of the particular set of polynomials which can be most easily demonstrated by choosing a particular order for the polynomials. Thus for the function vector $\vec{\psi}(\vec{r})$ in Eq. (19) we choose a complex twenty element vector.

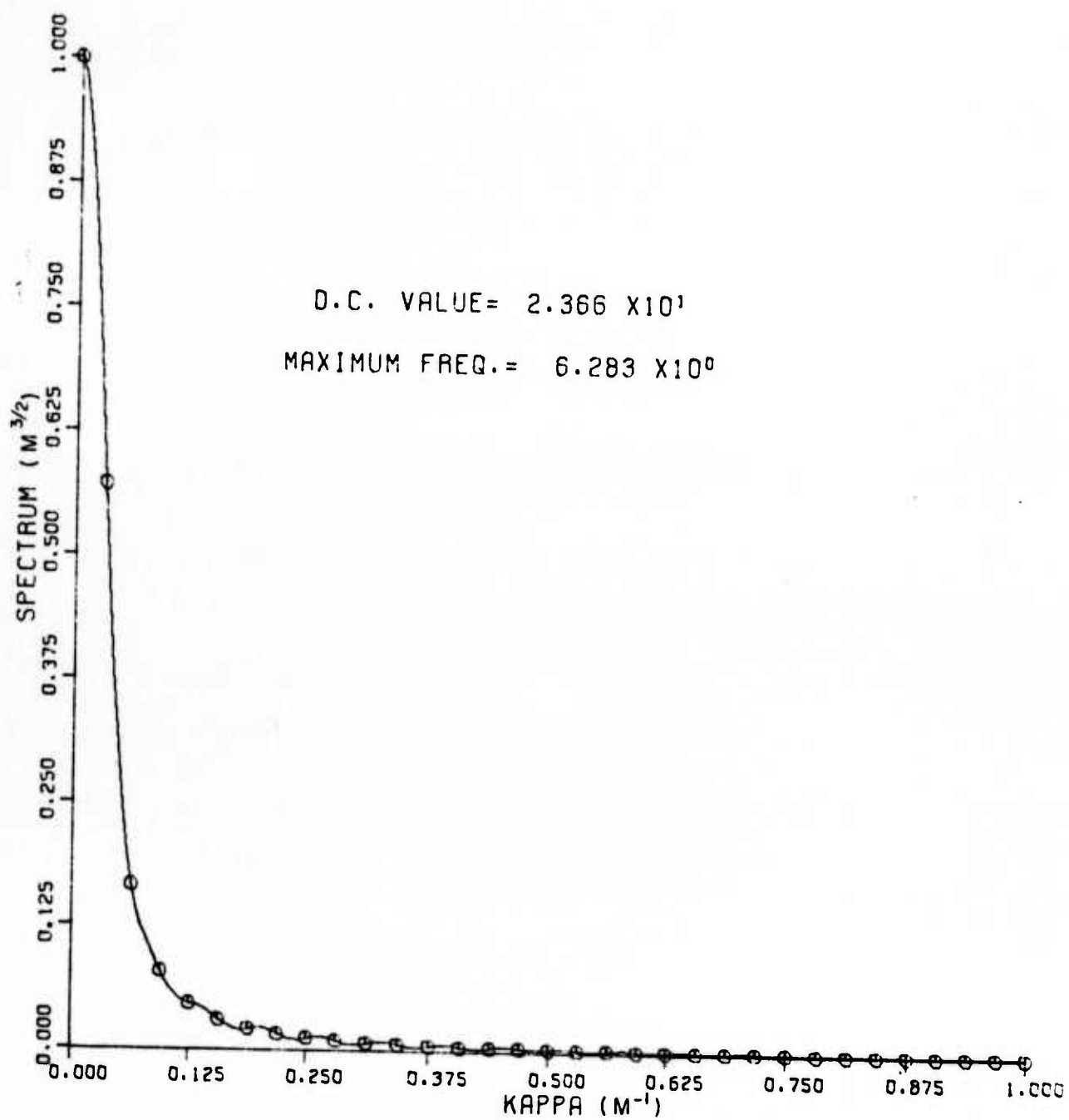


Fig. 4a. Linear plots of spectra F_a , F_b , and F_c for spectral regions $n=1$ and 2 . The negative of F_b and F_c are plotted.

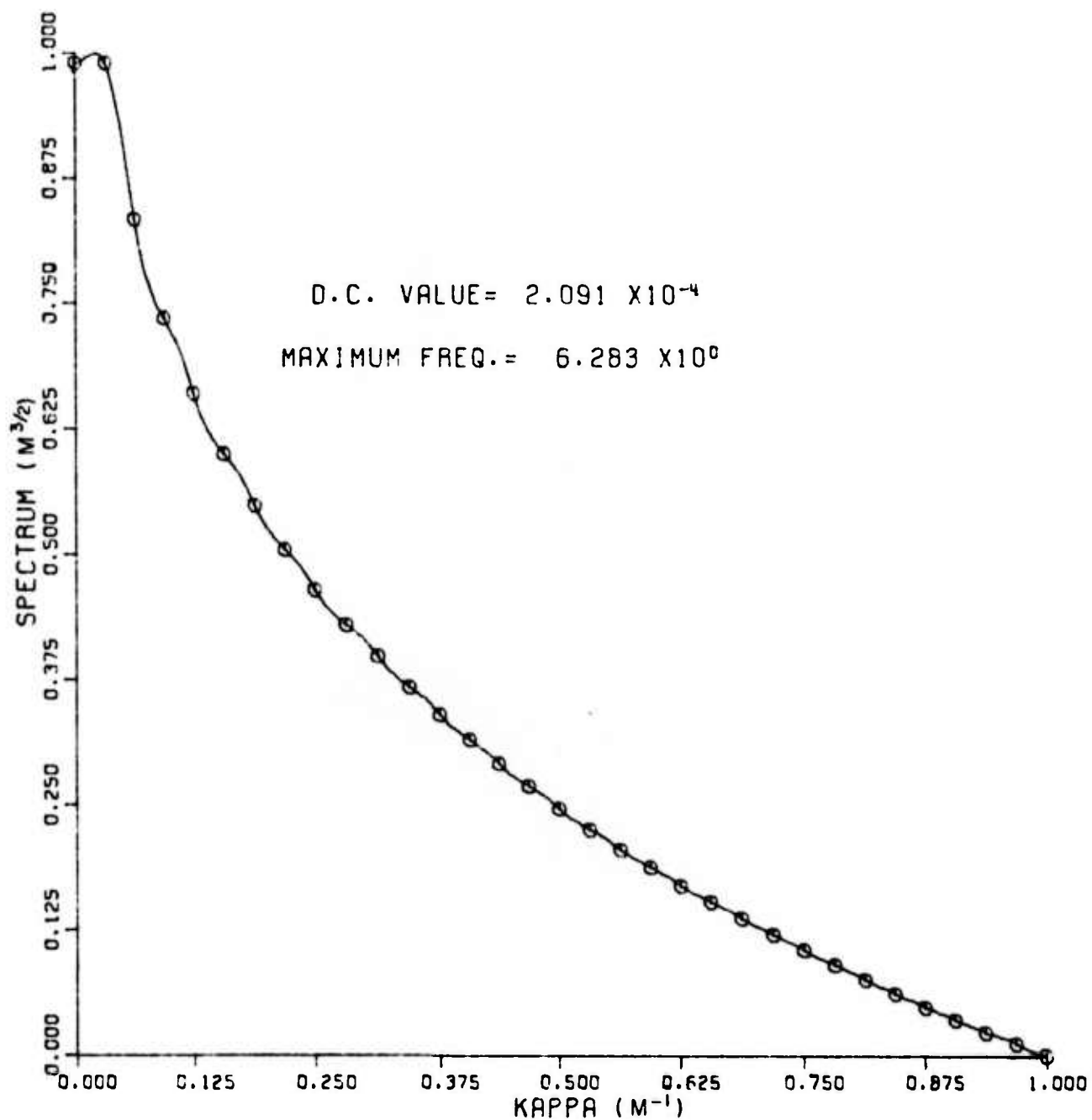


Fig. 4b. Linear plots of spectra F_a , F_b , and F_c for spectral regions $n=1$ and 2. The negative of F_b and F_c are plotted.

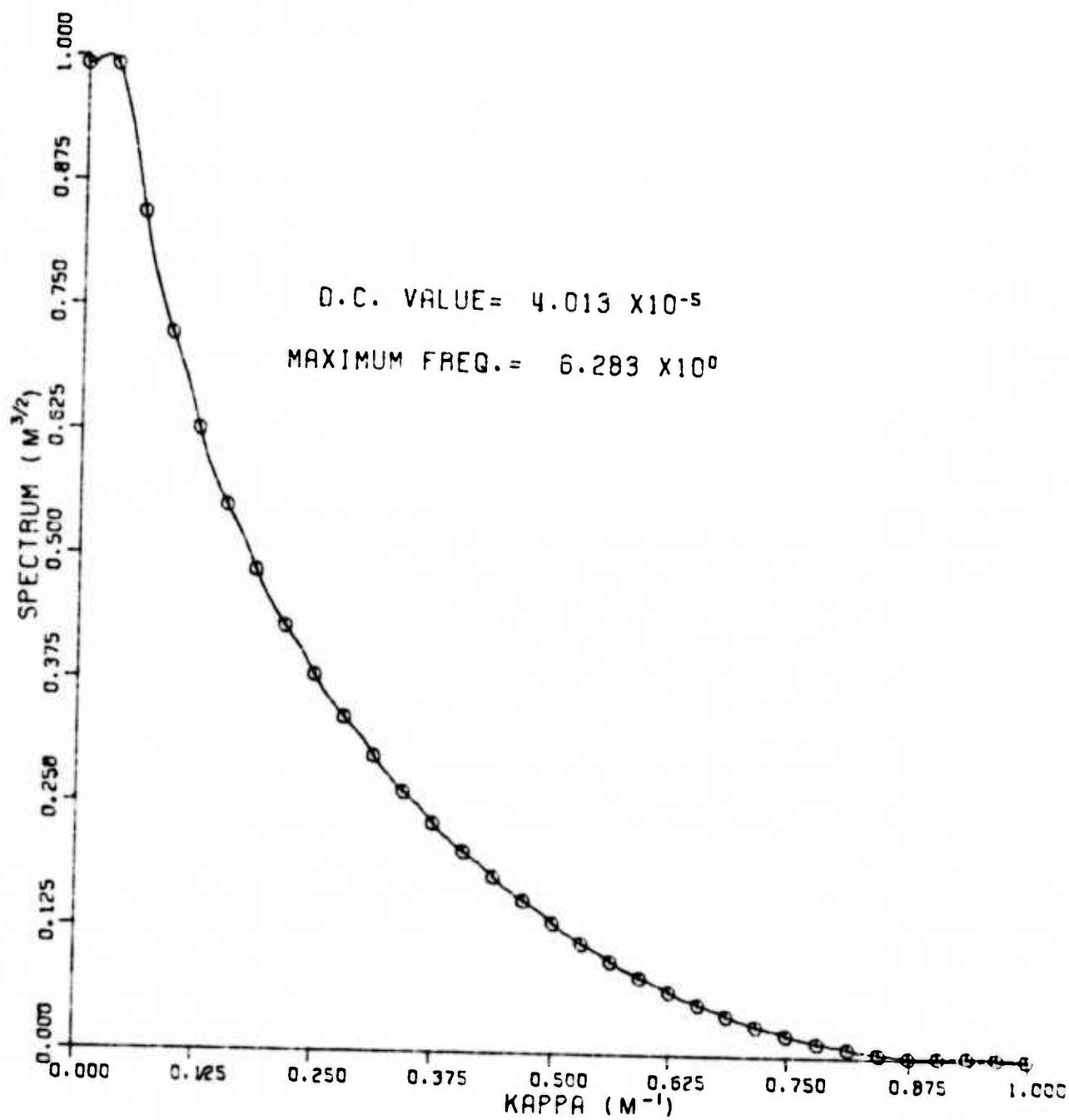


Fig. 4c. Linear plots of spectra F_a , F_b , and F_c for spectral regions $n=1$ and 2 . The negative of F_b and F_c are plotted.

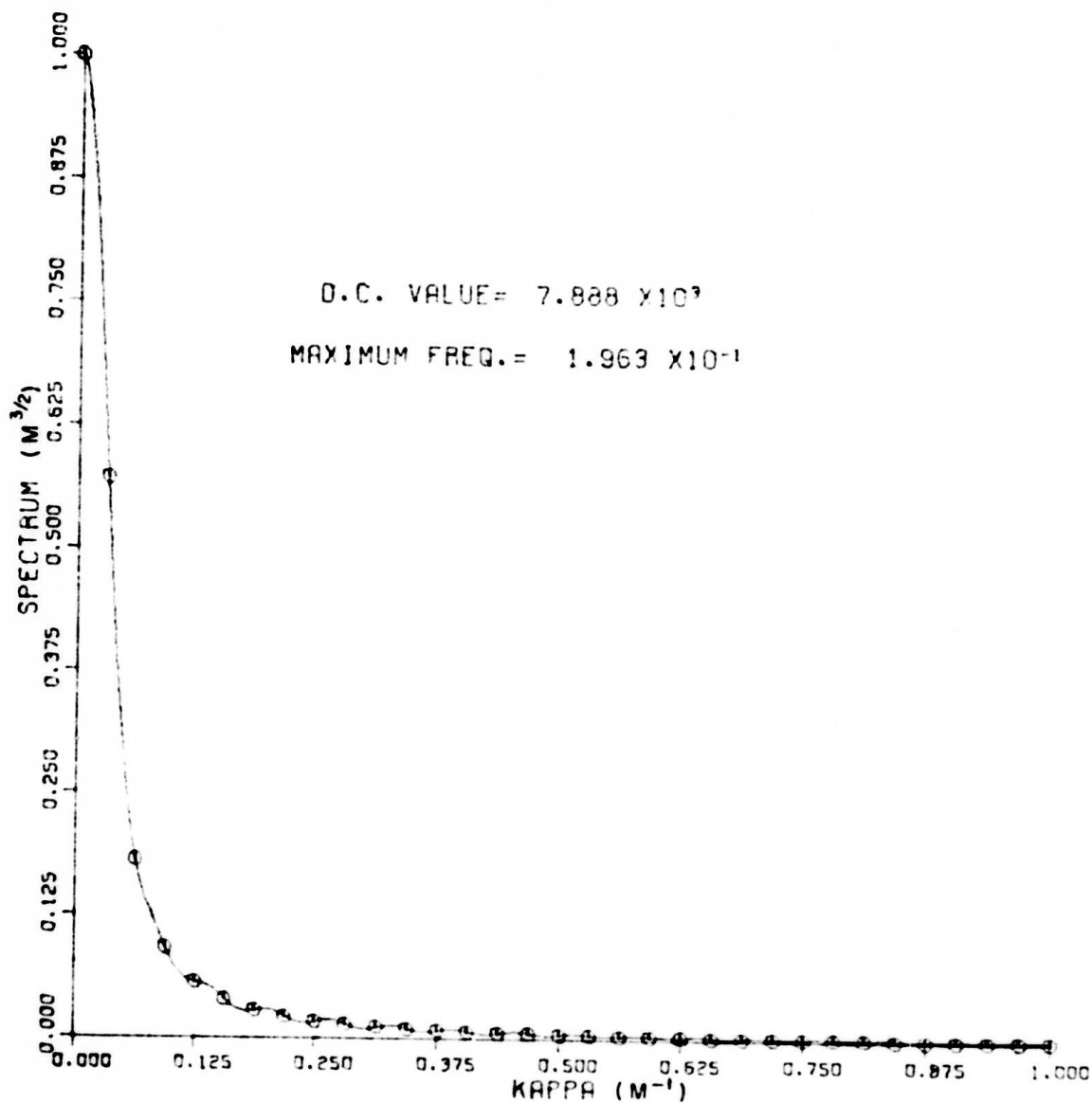


Fig. 4d. Linear plots of spectra F_a , F_b , and F_c for spectral regions $n=1$ and 2 . The negative of F_b and F_c are plotted.

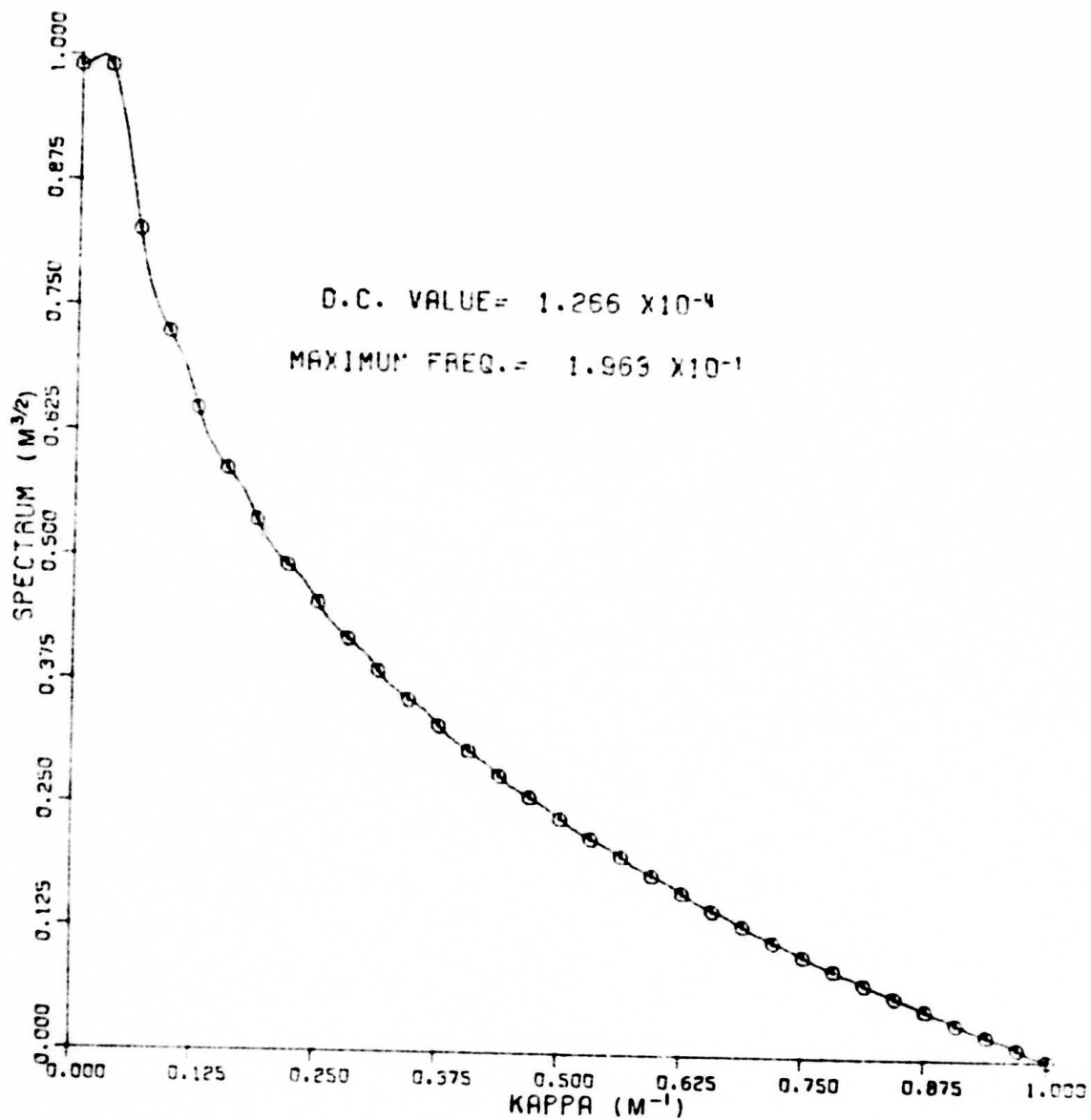


Fig. 4e. Linear plots of spectra F_a , F_b , and F_c for spectral regions $n=1$ and 2 . The negative of F_b and F_c are plotted.

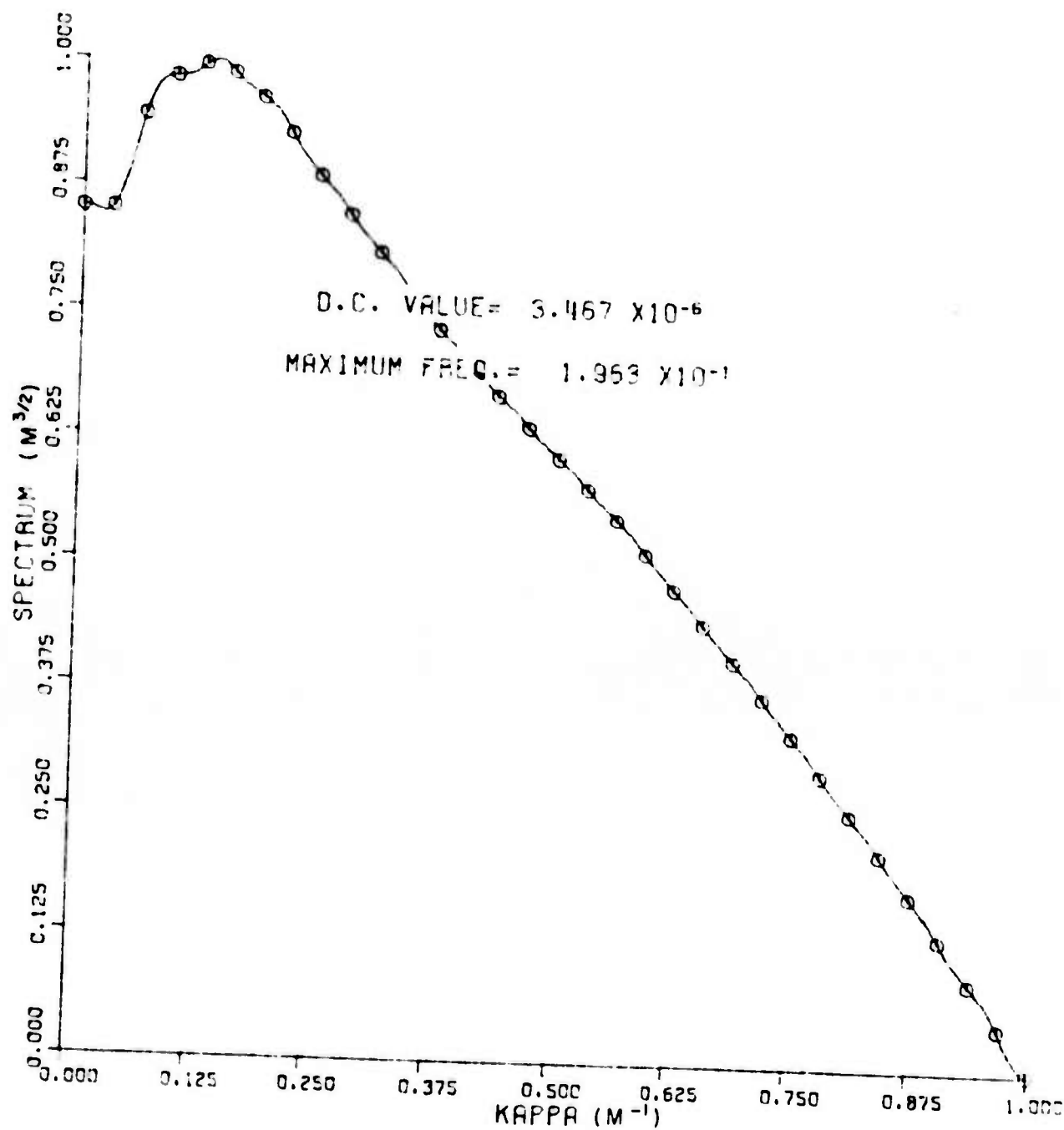


Fig. 4f. Linear plots of spectra F_a , F_b , and F_c for spectral regions $n=1$ and 2 . The negative of F_b and F_c are plotted.

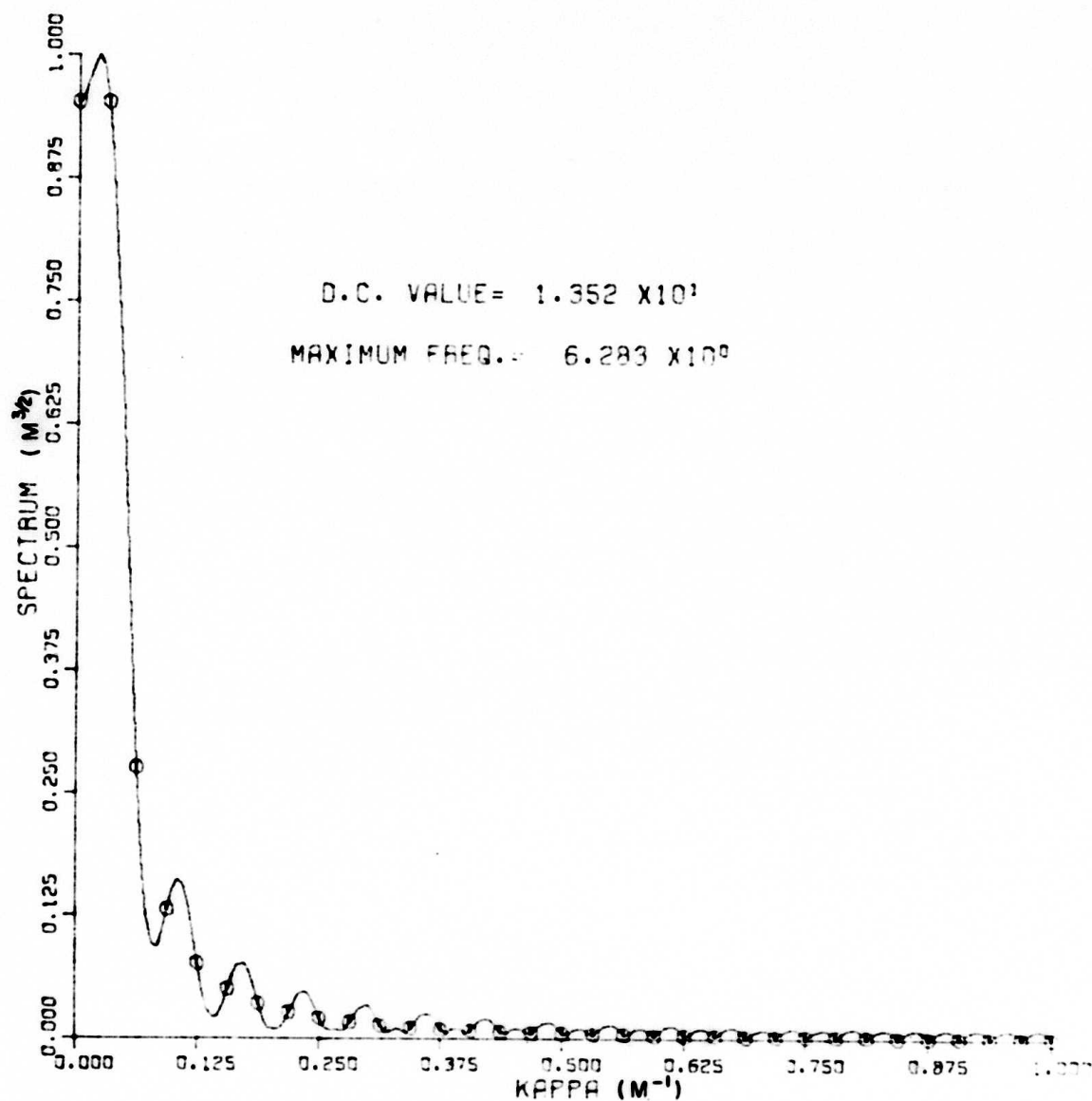


Fig. 4g. Linear plots of spectra F_a , F_b , and F_c for spectral regions $n=1$ and 2. The negative of F_b and F_c are plotted.

$$(32) \quad \psi(\bar{r}) (j\psi_0(\bar{r}), j\psi_3(\bar{r}), j\psi_4(\bar{r}), j\psi_5(\bar{r}), j\psi_1(\bar{r}), j\psi_6(\bar{r}), j\psi_8(\bar{r}), \\ j\psi_2(\bar{r}), j\psi_7(\bar{r}), j\psi_9(\bar{r}), \psi_0(\bar{r}), \psi_3(\bar{r}), \psi_4(\bar{r}), \psi_5(\bar{r}), \\ \psi_1(\bar{r}), \psi_6(\bar{r}), \psi_8(\bar{r}), \psi_2(\bar{r}), \psi_7(\bar{r}), \psi_9(\bar{r})).$$

The imaginary part is given first for later convenience in displaying the results.

The simplification is that the covariance matrix divides into simpler submatrices as shown in Eq. (33).

$$(33) \quad \bar{C} = \begin{array}{|c|c|c|c|} \hline \begin{array}{c} 6 \times 6 \\ \text{Group I} \end{array} & & & 0 \\ \hline & \begin{array}{c} 2 \times 2 \\ \text{II} \end{array} & & \\ \hline & & \begin{array}{c} 6 \times 6 \\ \text{Group III} \end{array} & \\ \hline 0 & & & \begin{array}{c} 6 \times 6 \\ \text{Group IV} \end{array} \\ \hline \end{array}$$

It might be noted that a covariance matrix of the form shown in Eq. (33) exists for each of the low frequency spectral regions.

The covariance matrices, eigenvalues and eigenvectors for spectral regions $n=1$ and $n=2$ are shown in Table I. The submatrices are divided into sections. The upper left and lower right quadrants contain phase and log-amplitude covariances respectively. The other two quadrants contain phase-log-amplitude cross-covariances.

The eigenvalues are listed in the next row in decreasing order. Below each eigenvalue is the corresponding eigenvector. It is interesting to note that the eigenvectors with one exception all contain one element very near unity and with the other elements smaller by at least several orders of magnitude. This indicates that for these eigenvalues: first there is very little cross-coupling between phase and log-amplitude, and second that the polynomials chosen are indeed quite reasonable representations of the actual eigenfunctions. The one exception is a mixing between the

consistant and spherical terms for $n=1$. The result is two intensity patterns neither of which is constant. It seems reasonable that a constant intensity would not be one of the "natural" patterns for atmospherically degraded light.

The adjusted spectra F_a , F_b , and F_c for the region $n=0$ are shown in Figs. 5. The two-dimensional integral of these are obtained and combined to form the variances of phase and log-amplitude. These variances are shown in Table 2 along with the sums of the eigenvalues for regions $n=1$ and 2. It is interesting that the phase variances for other than the constant term are larger than the phase variance in region $n=0$. The log-amplitude contribution of region $n=0$ is much larger than that from region $n=1$, thus indicating the "high pass" property of the atmosphere to amplitude fluctuations.

Figures 6 are contour plots made from a typical manifestation of a degraded wavefront. There we see the contributions from the regions $n=2, 1$ and 0. The contour lines are drawn every half wavelength for phase and every half radian for log amplitude. As expected the contours are more closely spaced in the high frequency regions. For lower spatial frequencies than $n=2$ the contribution is merely a constant and is not shown.

The results of Table II tend to indicate that the Fourier transform technique and the polynomial approach are both necessary and important in the complete description of light that has come down through the atmosphere. One might ask if the polynomial approach could be used to alone simulate atmospherically degraded wavefronts. To answer that question we consider some further results of a slightly different nature. The Karhunen-Loève integral equation was solved numerically using the correlation function derived from the phase spectrum of Fig. 2. A grid of eight by eight points was used. The eigenvalues are shown in Appendix D along with the designations of a few low order eigenfunctions. Reference to that appendix shows that the eigenvalues are very closely spaced in value indicating that it would be difficult to reject any of the eigenfunctions. Thus all sixty-four eigenfunctions would be necessary for the coarse grained eight by eight simulation. Even if all the eigenfunctions were used they would have to be summed at each point with random coefficients to generate the simulated wavefront. If all those random coefficients are going to be necessary it seems much more economical of time to use the Fourier transform technique to generate the wavefronts directly than to have to sum over each eigenfunction for every point desired. Thus for the high spatial frequency region the Fourier transform approach seems much more economical than the eigenfunction approach. On the other hand the polynomial approach requires many fewer terms in the lower spatial frequency region. The general conclusion then is that the combination is the appropriate one where both high and low frequencies are involved all together.

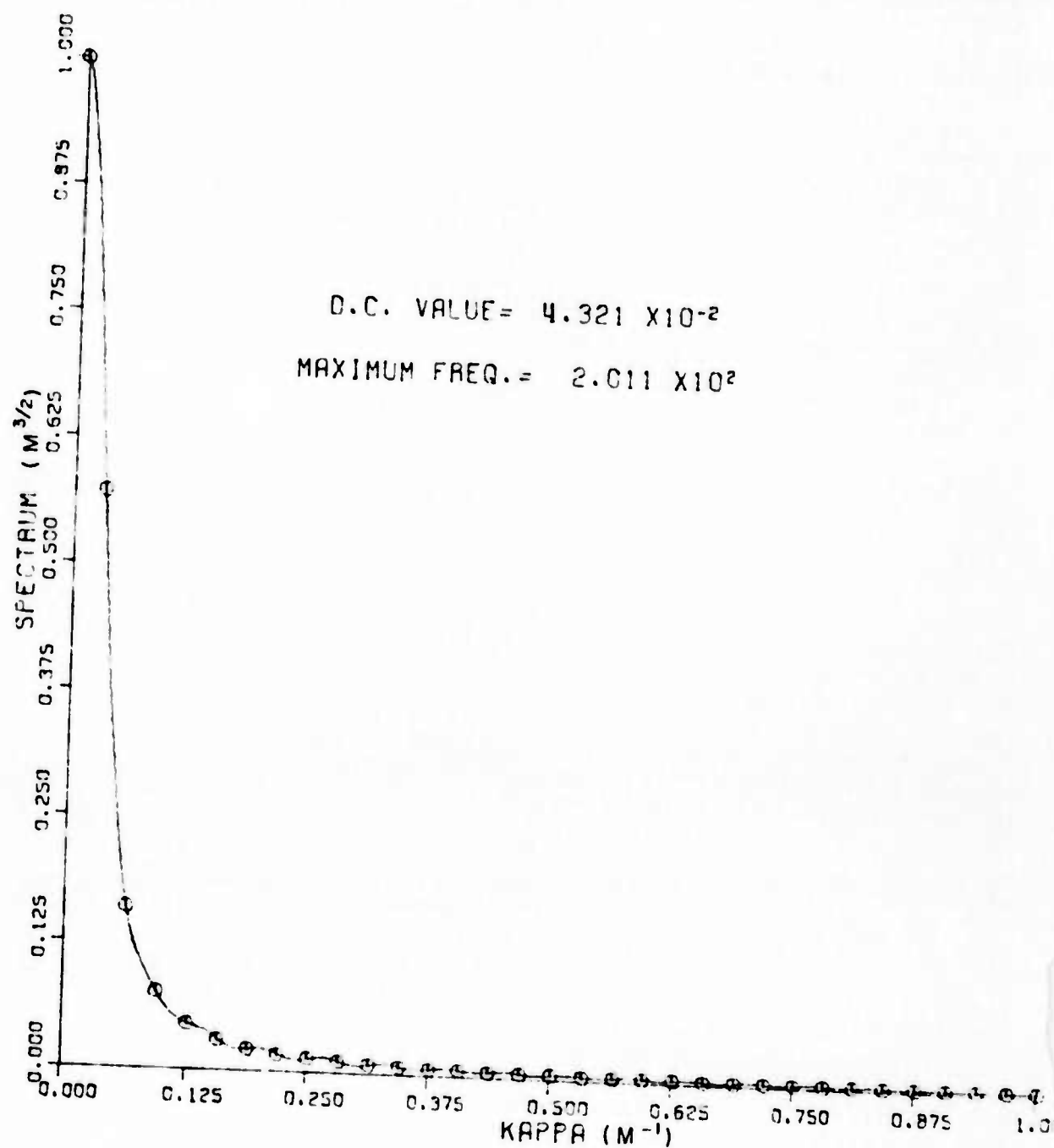


Fig. 5a. Linear plots of spectra F_a , F_b and F_c used in the spectral region $n=0$. The magnitude of F_c is plotted.

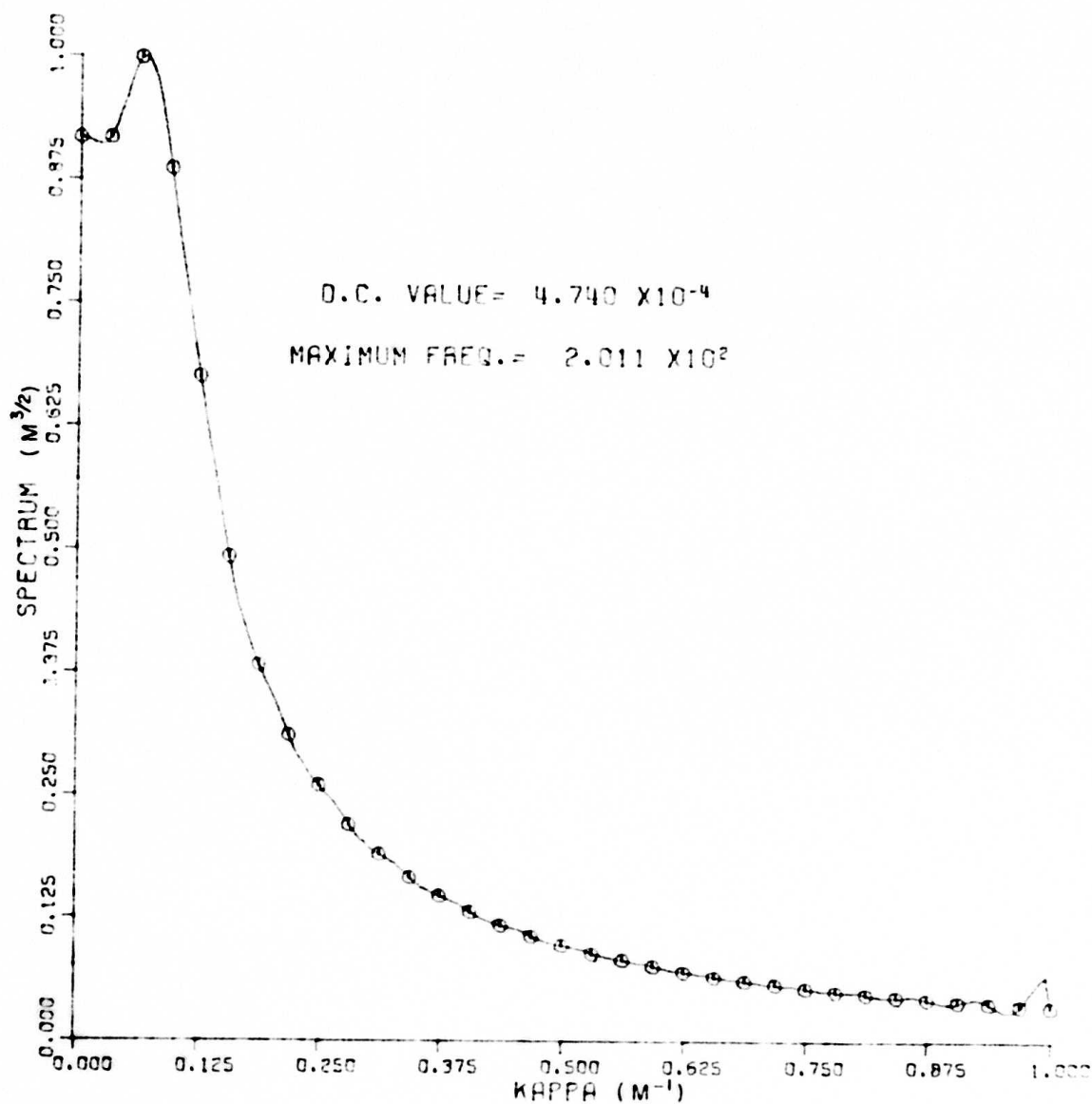


Fig. 5b. Linear plots of spectra F_a , F_b and F_c used in the spectral region $n=0$. The magnitude of F_c is plotted.

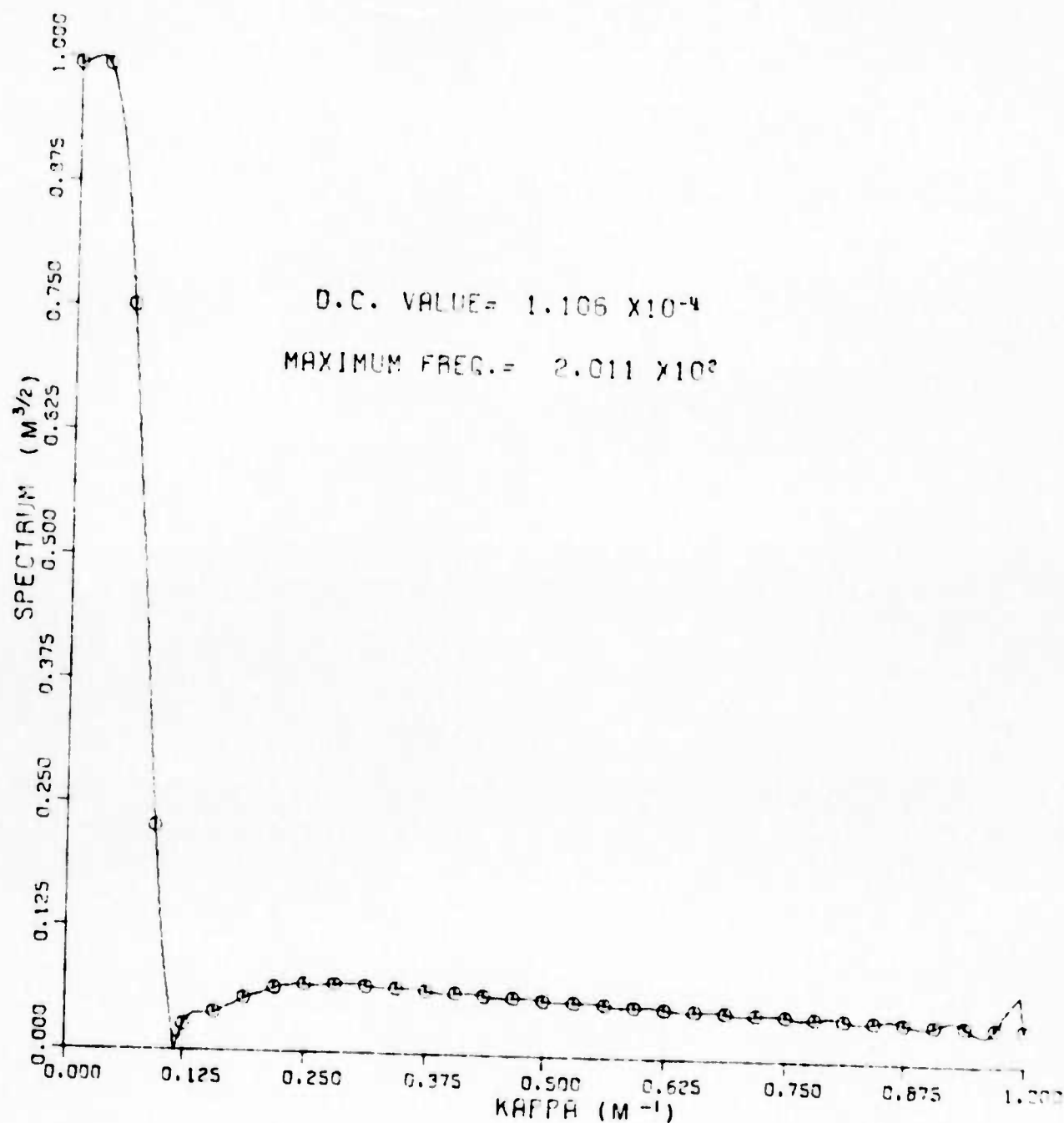


Fig. 5c. Linear plots of spectra F_a , F_b and F_c used in the spectral region $n=0$. The magnitude of F_c is plotted.

TABLE I

GROUP I. OC AND SPHERICAL. N=1

COVARIANCE MATRIX

.55180	2	-.15920	0	.00000	1	-.27530	-3	.48890	-5	.00000	1
-.15920	0	.95800	-2	-.52650	-11	.48890	-5	-.61050	-6	-.35600	-15
.00000	1	-.52650	-11	.53210	-2	.00000	1	-.35600	-15	-.33890	-6
-.27530	-3	.48890	-5	.00000	1	.17510	-6	-.17600	-7	.00000	1
.48890	-5	-.61050	-6	-.35600	-15	-.17600	-7	.55670	-8	-.43560	-17
.00000	1	-.35600	-15	-.33890	-6	.00000	1	-.43560	-17	.33320	-8

EIGENVALUES

.55180	2	.91210	-2	.53210	-2	.17180	-6	.55270	-8	.33110	-8
--------	---	--------	----	--------	----	--------	----	--------	----	--------	----

EIGENVECTORS

.10000	1	.28650	-2	.00000	1	.36940	-5	.10000	-6	.00000	1
-.28650	-2	.10000	1	.00000	1	-.44890	-3	.65390	-4	.00000	1
.00000	1	.00000	1	.10000	1	.00000	1	.00000	1	.63700	-4
-.49890	-5	.44690	-3	.00000	1	.10000	1	.29350	-7	.00000	1
.88630	-7	-.65390	-4	.00000	1	.00000	1	.10000	1	.00000	1
.00000	1	.00000	1	-.63700	-4	.00000	1	.00000	1	.10000	1

GROUP II. HYPERBOLIC. N=1

COVARIANCE MATRIX

.11790	-1	-.72020	-6
-.72020	-6	.70920	-8

EIGENVALUES

.11790	-1	.70480	-8
--------	----	--------	----

EIGENVECTORS

.10000	1	.61100	-4
-.61100	-4	.10000	1

TABLE I

GROUPS III, IV, LINEAR AND CURVIC. N=1

COVARIANCE MATRIX

.25640	0	-.40830	-2	-.46980	-2	-.80090	-5	.25710	-6	.30490	-6
-.40830	-2	.10790	-1	.25510	-3	.25710	-6	-.12840	-6	-.13050	-7
-.48980	-2	.25510	-3	.43450	-3	.30490	-6	-.13050	-7	-.27330	-7
-.80090	-5	.25710	-6	.30490	-6	.30750	-7	-.22750	-8	-.27410	-8
.25710	-6	-.12840	-6	-.13050	-7	-.22750	-8	.16860	-7	.29410	-9
.30490	-6	-.13050	-7	-.27330	-7	-.27410	-8	.29410	-9	.46140	-9

EIGENVALUES

.25660	0	.10720	-1	.33780	-3	.31040	-7	.16490	-7	.21530	-9
--------	---	--------	----	--------	----	--------	----	--------	----	--------	----

EIGENVECTORS

.99970	0	.16950	-1	.16850	-1	.22390	-4	.31620	-5	.20150	-5
-.16630	-1	.99970	0	-.17050	-1	-.64610	-5	.10390	-4	-.85920	-6
-.19130	-1	.16750	-1	.99970	0	-.44420	-3	-.53230	-4	.23760	-4
-.31240	-4	.11790	-4	.44260	-3	.96320	0	.16020	0	.87890	-1
.10110	-5	-.11590	-4	-.17790	-4	-.15960	0	.98710	0	-.14260	-1
.11910	-5	-.77750	-6	-.63200	-4	-.89040	-1	.13790	-16	.99400	0

TABLE I

GROUP I, OC AND SPHERICAL, N=2

COVARIANCE MATRIX									
.20680	6	-.10360	1	.00000	1	-.53480	-3	.42050	-7
-.10360	1	.13560	-3	-.65670	-13	.42050	-7	-.19890	-10
.00000	1	-.65670	-13	.54580	-4	.00000	1	-.68150	-20
-.53480	-3	.42050	-7	.00000	1	.27900	-8	-.48730	-12
.42050	-7	-.19890	-10	-.68150	-20	-.48730	-12	.29190	-15
.00000	1	-.68150	-20	-.51180	-11	.00000	1	-.98090	-25
EIGENVALUES									
.20680	6	.13040	-3	.54580	-4	.27880	-8	.29190	-15
EIGENVECTORS									
.10000	1	.40110	-5	.00000	1	.25860	-8	.00000	1
-.50110	-5	.10000	1	.00000	1	-.12960	-13	.00000	1
.00000	1	.00000	1	.10000	1	.00000	1	.00000	1
-.25860	-8	.00000	1	.00000	1	.10000	1	.00000	1
.00000	1	.00000	1	.00000	1	.00000	1	.10000	1
.00000	1	.00000	1	.00000	1	.00000	1	.00000	1
EIGENVALUES									
.20680	6	.13040	-3	.54580	-4	.27880	-8	.29190	-15
EIGENVECTORS									
.10000	1	.40110	-5	.00000	1	.25860	-8	.00000	1
-.50110	-5	.10000	1	.00000	1	-.12960	-13	.00000	1
.00000	1	.00000	1	.10000	1	.00000	1	.00000	1
-.25860	-8	.00000	1	.00000	1	.10000	1	.00000	1
.00000	1	.00000	1	.00000	1	.00000	1	.10000	1
.00000	1	.00000	1	.00000	1	.00000	1	.00000	1

GROUP II, HYPERBOLIC, N=2

COVARIANCE MATRIX									
.16840	-3	-.23990	-10						
-.23990	-10	.34800	-15						
EIGENVALUES									
.16840	-3	.34800	-15						
EIGENVECTORS									
.10000	1	.14250	-6						
-.14250	-6	.10000	1						

TABLE I

GROUPS III AND IV. LINEAR AND CURIC, N=2

COVARIANCE MATRIX										
.16360	1	-.56910	-4	-.59730	-4	-.63340	-7	.10790	-10	
-.56910	-4	.49620	-6	.10930	-7	.10790	-10	-.11300	-12	
-.59730	-4	.10930	-7	.76630	-8	.68740	-11	-.30500	-14	
-.63340	-7	.10790	-10	.68740	-11	.71870	-12	-.16050	-15	
.10790	-10	-.11300	-12	-.30500	-14	-.16050	-15	.17980	-17	
.68740	-11	-.30500	-14	-.14380	-14	-.95810	-16	.48450	-19	
								.21660	-19	
EIGENVALUES										
.16360	1	.59570	-6	.52980	-6	.71620	-12	.17980	-17	
									.21660	-19
EIGENVECTORS										
.10000	1	.41690	-4	.35620	-4	.38720	-7	.00000	1	
-.40900	-4	.99960	0	-.21740	-1	-.15840	-11	.00000	1	
-.36520	-4	.21740	-1	.99980	0	-.14140	-11	.00000	1	
-.58720	-7	.00000	1	.00000	1	.10000	1	.00000	1	
.00000	1	.00000	1	.00000	1	.00000	1	.10000	1	
.00000	1	.00000	1	.00000	1	.00000	1	.00000	1	
								.10000	1	



Fig. 6a. Contour plots of the contributions from spectral regions $n=0$, 1, and 2 to phase front and log-amplitude front.

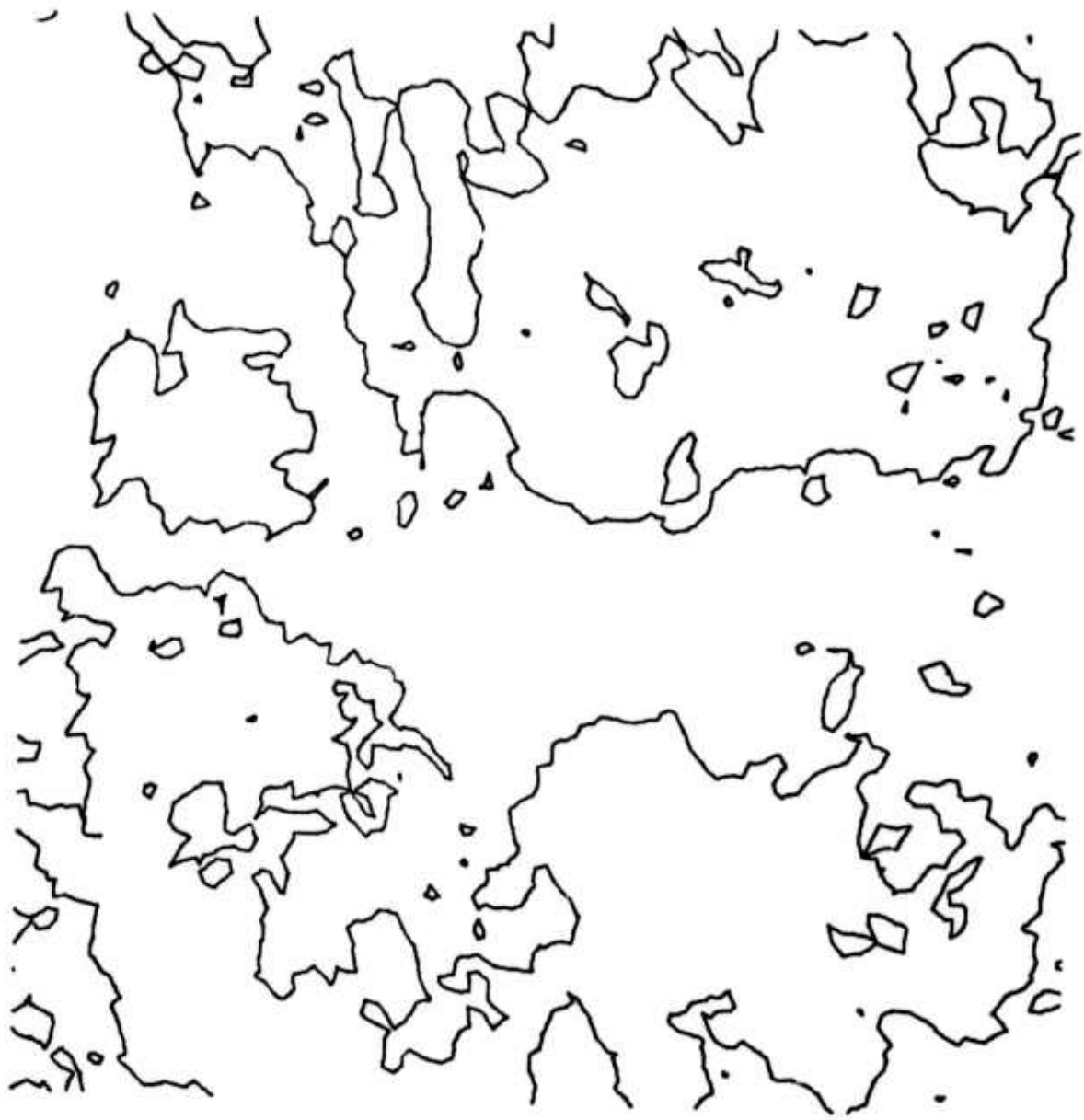


Fig. 6b. Contour plots of the contributions from spectral regions $n=0$, 1, and 2 to phase front and log-amplitude front.



Fig. 6c. Contour plots of the contributions from spectral regions $n=0$, 1 , and 2 to phase front and log-amplitude front.

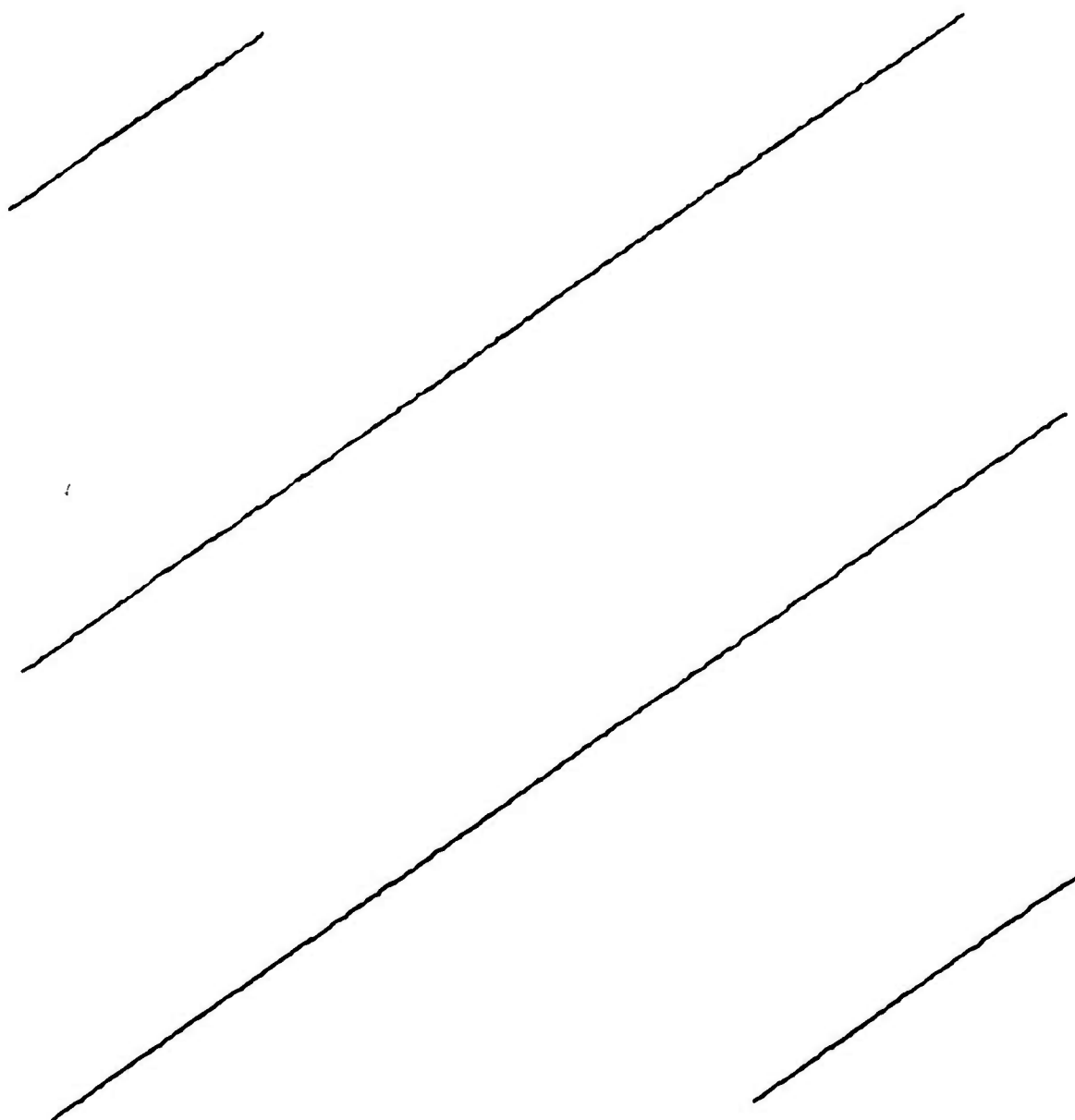


Fig. 6d. Contour plots of the contributions from spectral regions $n=0$, 1, and 2 to phase front and log-amplitude front.

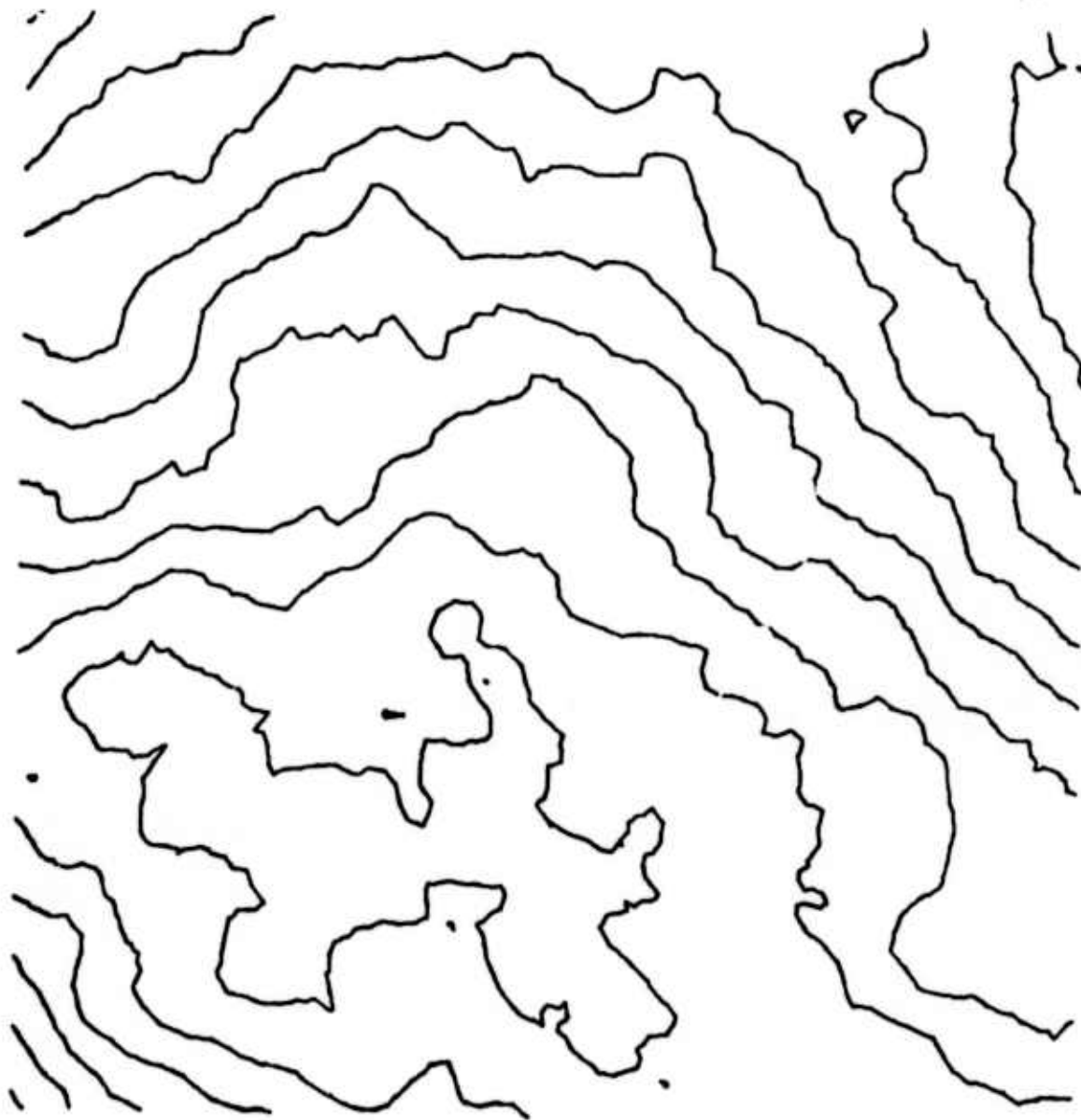


Fig. 6e. Contour plots of the contributions from spectral regions $n=0$, 1, and 2 to phase front and log-amplitude front.

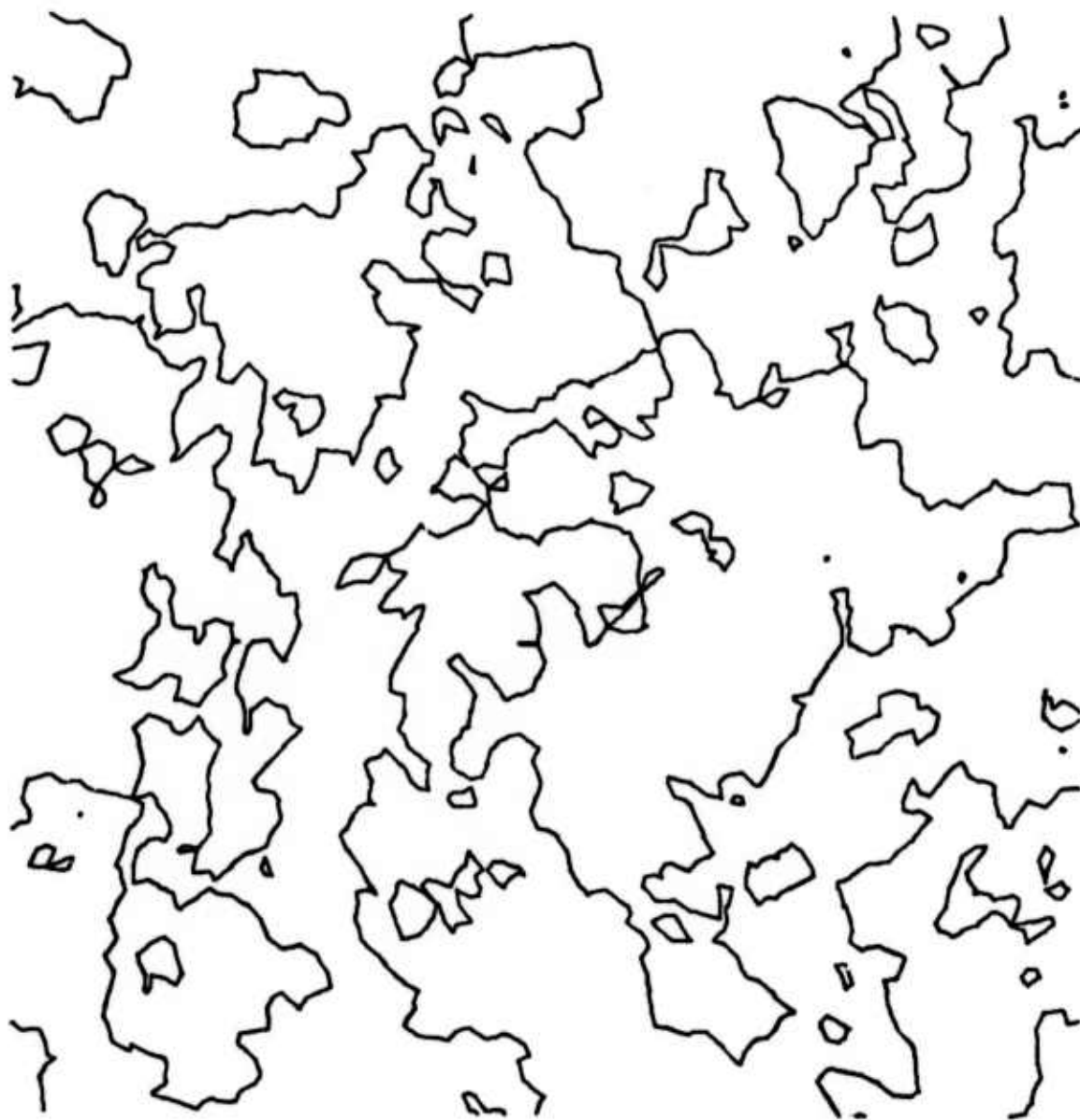


Fig. 6f. Contour plots of the contributions from spectral regions $n=0$, 1, and 2 to phase front and log-amplitude front.

TABLE II

n	Variance	
	Phase	Log-amplitude
0	.2220	$.3017 \times 10^{-3}$
1	$.5543 \times 10^2$	$.9330 \times 10^{-6}$
2	$.2068 \times 10^6$	$.2788 \times 10^{-8}$

One other item might be mentioned in passing. In the application of the polynomial scheme it is required that the eigenvalues be positive if the scheme is to be used for wavefront simulation because the random coefficients are scaled by the square root of the eigenvalue. This requires that the covariance matrix be positive-definite. In the scheme for splitting the spectra into regions there is no obvious way of assuming that the new spectra thus generated will lead to positive-definite matrices. In the case at hand it has worked out that way and perhaps always will. The method of relating the usual requirement for positive definiteness, that all the sub determinants be positive, to the spectra is not obvious. More work could be done on this point.

Finally after the new spectra have been computed for region $n=0$, and the eigenfunctions and eigenvalues have been obtained for regions $n=1 \dots 4$ we can actually generate the random wavefronts. This is done using Eqs. (5) and (9) for the highest spectral region and Eq. (22) for the lower spectral regions. The procedure is illustrated in the computer algorithm shown in Fig. 7.

To summarize, in this section the complete wavefront simulation scheme was illustrated for the spectra under consideration. A set of polynomials was chosen for the low frequency spectral regions, and the covariance matrix diagonalized to give the Karhunen-Loève polynomials appropriate for uncorrelated random coefficients. A complete wave-front was illustrated in terms of the contributions from the various spectral regions.

6. SUMMARY

To summarize, we have developed a scheme for simulating randomly degraded optical beams including both phase and log-amplitude and the effect of their cross-correlation. The scheme works for optical degradations whose scale lengths range from much smaller to much larger than the input aperture size. An extension of the well-known Fourier transform method is used for the small scale fluctuations and a polynomial approach is used for the larger scale fluctuations.

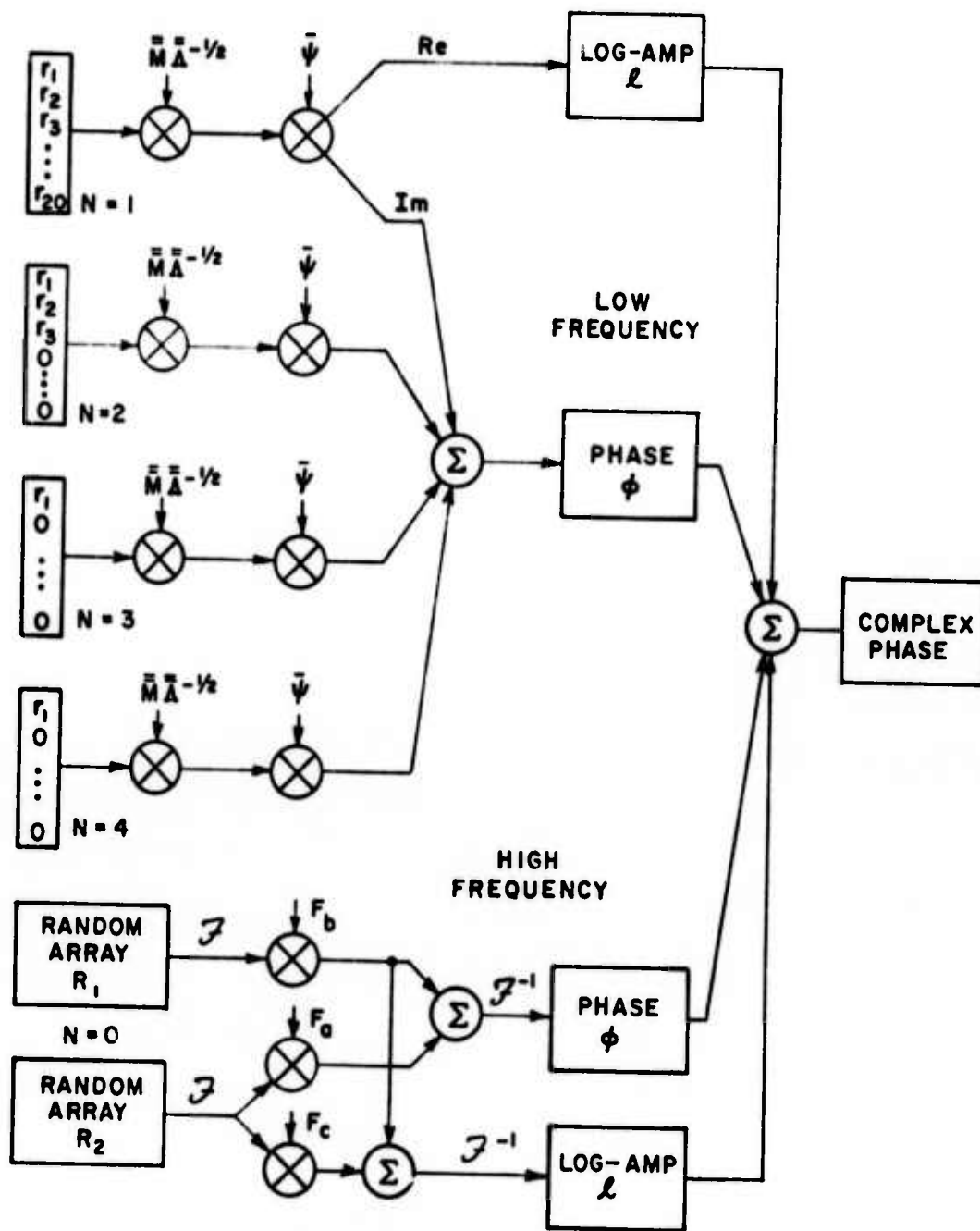


Fig. 7. Schematic diagram of computer wavefront generation algorithm.

In the report Section 2 contains a discussion of the physical situation. This is characterized by a large range of scale sizes for the fluctuations; a difficult problem for the Fourier transform procedure alone because a prohibitively large array would be required. The spatial spectrum is split into regions, the contribution to the degraded optical beam from each spectral region to be computed separately. Treated in Section 3 is the highest spatial frequency region in which the Fourier transform approach is used. In this section the mathematical formalism for using the Fourier transform approach to generate both phase and log-amplitude fluctuations including their correlation is derived. In Section 4 the contributions from the lower spatial frequency regions are considered. These are generated using a polynomial approach. The procedure for finding the set of polynomials which could be used with the uncorrelated random numbers that can be easily generated by a digital computer is worked out. It is shown in Appendix B that the procedure is formally identical to the Karhunen-Loève procedure.

In Section 5 the procedures developed in Sections 2, 3, and 4 are demonstrated in the simulation of an optical beam that has come down through the atmosphere. The spatial spectral division is illustrated and a particular set of orthonormal polynomials is transformed into the polynomials appropriate for uncorrelated random coefficients. The Fourier transform technique is used for the highest frequency portion of the spatial spectrum. Finally a sample composite wavefront is illustrated, showing the relative contributions from the various frequency ranges.

7. CONCLUSIONS

The problem considered initially in this project was to find a technique for the computer simulation of randomly degraded optical beams including phase and log-amplitude fluctuations. In the process two approaches were to be considered, the Fourier transform approach used previously by others and the Karhunen-Loève polynomial approach.

We can conclude that a technique has been found. It is to first find spatial spectra that can be combined to give phase and log-amplitude; second to split these spectra into regions, each with its own spectra; and third to find the contributions to the wave front from each spectral region. An extension of the Fourier transform technique is used in the highest spectral region while a polynomial scheme is used in the lower frequency regions. The technique is one which makes efficient use of computer time because a polynomial approach is used to simulate the effects of the large scale fluctuations which vary more slowly over the input aperture and the Fourier transform procedure is used where it is best suited in the simulation of small scale fluctuations.

During the process of developing this wavefront simulation algorithm several other problems were solved. The problem of using the Fourier transform method to simulate both phase and log-amplitude fluctuations including their cross-correlation was solved. The problem of using the Karhunen-Loève approach for wavefront simulation was considered and extended to a complex variable, the complex log-amplitude, thus enabling the application of that approach to both phase and log-amplitude. A problem of handling the large range of spatial scale sizes was solved by the spatial frequency division. Further the problem was solved using an efficient scheme by combining the Fourier transform approach and the polynomial approach for ranges where they can be most suitably used. This technique will be especially useful in the computer examination of active systems to be used for the compensation of atmospheric degradation of images (satellite, etc.) the light for which has propagated large distances down through the atmosphere.

APPENDIX A SPECTRA

In this appendix we derive the expressions for the spatial spectra of phase and log-amplitude covariances and the phase-log amplitude cross covariance for light that has propagated down through the atmosphere. The expressions draw upon work in the literature (Tatarski, 1971) and end up with computer evaluation of the associated integral expressions. In this case the spectra are particularly significant because they apply to a light beam which has propagated down through the atmosphere where there is a much larger low spatial frequency content than for light propagated horizontally near the ground.

The starting point for the three spectra are expressions in the literature (Tatarski, 1971, Eqs. 5-27, 5-33, 46-14, 15, 16, and 46-22, 23, 25, 26).

$$(1a) F_1(\bar{r}_T, L) = k^2 \int_0^L \int_0^L \exp \frac{j \bar{r}_T^2 (z' - z'')}{2k} F_n(\bar{k}_T, z' - z'') dz' dz''$$

$$(1b) F_2(\bar{r}_T, L) = -k^2 \int_0^L \int_0^L \exp \frac{-j \bar{r}_T^2 (2L - z' - z'')}{2k} F_n(\bar{r}_T, z' - z'') dz' dz''$$

$$(1c) F_{\pm} = \frac{1}{2} [F_1 + \text{Re}(F_2)]$$

$$(1d) F_{\pm} = \frac{1}{2} [F_1 - \text{Re}(F_2)]$$

$$(1e) F_{\pm} = \frac{1}{2} \text{Im } F_2$$

$$(1f) B_{\pm}(\beta) = 2\pi \int_0^{\infty} J_0(\beta r) F_{\pm}(\bar{r}_T, L) \cdot \bar{r}_T d\bar{r}_T$$

$$(1g) F_n(\bar{\kappa}_T, z' - z'') = \int_{-\infty}^{\infty} \phi_n(\bar{\kappa}) e^{j\kappa_z(z' - z'')} d\kappa_z$$

where α stands for x, y , or z , and $\bar{\kappa}_T = (\kappa_x, \kappa_y)$ is the transverse component of $\bar{\kappa}$. In Eqs. (1) we are considering a plane wave propagating in the z direction from $z=0$ to $z=L$ so that z' and z'' are two points along the path. $\lambda = 2\pi/k$ is the light wavelength, and $\phi_n(\bar{\kappa}, z)$ is the refractive index spatial spectrum. We also assume that the index spectrum is a slowly varying function of mean position, $(1/2)(z' + z'')$ along the path.

As a first step in evaluating the integrals in Eqs. (1) we switch to sum and difference coordinates arranging the integration limits in such a way as to perform the difference coordinate integration first,

$$(2a) \quad \xi = z' - z'' \qquad z' = \eta + \frac{1}{2} \xi$$

$$(2b) \quad \eta = \frac{z' + z''}{2} \qquad z'' = \eta - \frac{1}{2} \xi$$

Combining Eqs. (2), (1a), and (1g), gives

$$(3) \quad F_1(\bar{\kappa}_T, L) = k^2 \int_0^{L/2} d\eta \int_{-2\eta}^{2\eta} d\eta \, e^{\frac{j\kappa_T^2 \xi}{2k}} \int_{-\infty}^{\infty} d\kappa_z \phi_n(\bar{\kappa}, \eta) e^{i\kappa_z \xi} \\ + k^2 \int_{L/2}^L d\eta \int_{-2(L-\eta)}^{2(L-\eta)} d\eta \, e^{\frac{j\kappa_T^2 \xi}{2k}} \int_{-\infty}^{\infty} d\kappa_z \phi_n(\bar{\kappa}, \eta) e^{i\kappa_z \xi}$$

Performing the ξ integration, making the substitution $\eta' = L - \xi$ in the second integral and combining the integrals results in

$$(4a) F_1(\bar{\kappa}_T, L) = 4k^2 \int_0^{L/2} \eta d\eta \int_{-\infty}^{\infty} d\kappa_z \text{sinc} \left[2\eta \left(\frac{\kappa_T^2}{2k} + \kappa_z \right) \right]$$

$$\{ \phi_n(\bar{\kappa}, \eta) + \phi_n(\bar{\kappa}, L-\eta) \}$$

In Eqs. (4a), by definition, $\text{sinc}(x) = \sin(x)/x$. Performing similar operations on the F_2 integral gives

$$(4b) F_2(\bar{\kappa}_T, L) = -4k^2 \int_0^{L/2} \eta d\eta \int d\kappa_z \text{sinc}(2\eta \kappa_z) \left(\phi_n(\bar{\kappa}, \eta) e^{\frac{-i\kappa_T^2(L-\eta)}{k}} + \phi_n(\bar{\kappa}, L-\eta) e^{\frac{-i\kappa_T^2 \eta}{k}} \right)$$

We assume a von Karman type of refractive index spectrum where both the structure parameter, C_n^2 and the outer scale, L_0 are functions of height h given by Eqs. (5)

$$(5a) \phi_n(\kappa, \eta) = 0.033 C_n^2(\eta) \left(\left(\frac{1.077}{L_0(\eta)} \right)^2 + \kappa^2 \right)^{-11/6}$$

$$(5b) C_n^2(h) = C_n^2(H_0) (h/H_0)^{-4/3}$$

$$(5c) L_0(h) = L_0(H_0) (h/H_0)$$

We are considering downward propagation from height H_1 to height H_0 so that the height is related to the path variable, η , by

$$h = H_L - (H_L - H_0)(\eta/L) .$$

H_0 is the height at the bottom of the path so that

$$c_n^2(\eta) = c_n^2(H_0) \left(\frac{H_L}{H_0} - \frac{\eta}{L} \left(\frac{H_L}{H_0} - 1 \right) \right)^{-4/3}$$

$$L_0(r_i) + L_0(H_0) \left(\frac{H_L}{H_0} - \frac{\eta}{L} \left(\frac{H_L}{H_0} - 1 \right) \right)$$

Combining Eqs. (1c), (1d), (4a), (5), and (6) we have for F_ℓ , F_ϕ , and $F_{\ell\phi}$:

$$(7a) F_\ell = 2k^2 \times 0.033 c_n^2(H_0) \int_0^{L/2} \eta d\eta \int_{-\infty}^{\infty} d\kappa_z$$

$$\times \frac{\left(\frac{H_L}{H_0} - \frac{\eta}{L} \left(\frac{H_L}{H_0} - 1 \right) \right)^{-4/3} \left(\text{sinc}\left(2\eta \left(\frac{\kappa_T^2}{2k} + \kappa_z \right)\right) - \text{sinc}(2\eta\kappa_z) \cos\left(\frac{\kappa_T^2}{k} (L-\eta)\right) \right)}{\left(\left(\frac{1.077}{L_0(H_0) \left(\frac{H_L}{H_0} - \frac{\eta}{L} \left(\frac{H_L}{H_0} - 1 \right) \right)} \right)^2 + \kappa_T^2 + \kappa_z^2 \right)^{11/6}}$$

$$+ \frac{\left(\frac{H_L}{H_0} - \frac{(L-\eta)}{L} \left(\frac{H_L}{H_0} - 1 \right) \right)^{-4/3} \left(\text{sinc}\left(2\eta \left(\frac{\kappa_T^2}{2k} + \kappa_z \right)\right) - \text{sinc}(2\eta\kappa_z) \cos\left(\frac{\kappa_T^2}{k} \eta\right) \right)}{\left(\left(\frac{1.077}{L_0(H_0) \left(\frac{H_L}{H_0} - \frac{(L-\eta)}{L} \left(\frac{H_L}{H_0} - 1 \right) \right)} \right)^2 + \kappa_T^2 + \kappa_z^2 \right)^{11/6}}$$

$$(7b) F_{\phi} = 2k^2 \times 0.033 C_n^2(H_0) \int_0^{L/2} n d\eta \int_{-\infty}^{\infty} d\kappa_z$$

$$\times \left[\frac{\left(\frac{H_L}{H_0} - \frac{\eta}{L} \left(\frac{H_L}{H_0} - 1 \right) \right)^{-4/3} \left(\text{sinc} \left(2 \frac{\kappa_T^2}{2k} + \kappa_z \right) \right) + \text{sinc}(2\eta\kappa_z) \cos \left(\frac{\kappa_T^2}{k} (L-\eta) \right)}{\left(\left(\frac{1.077}{L_0(H_0) \left(\frac{H_L}{H_0} - \frac{\eta}{L} \left(\frac{H_L}{H_0} - 1 \right) \right)} \right)^2 + \kappa_T^2 + \kappa_z^2 \right)^{11/6}} \right. \\ \left. + \frac{\left(\frac{H_L}{H_0} - \frac{(L-\eta)}{L} \left(\frac{H_L}{H_0} - 1 \right) \right)^{-4/3} \left(\text{sinc} \left(2\eta \frac{\kappa_T^2}{2k} + \kappa_z \right) \right) + \text{sinc}(2\eta\kappa_z) \cos \left(\frac{\kappa_T^2}{k} \eta \right)}{\frac{1.077}{L_0(H_0) \left(\frac{H_L}{H_0} - \frac{(L-\eta)}{L} \left(\frac{H_L}{H_0} - 1 \right) \right)}^2 + \kappa_T^2 + \kappa_z^2)^{11/6}} \right]$$

$$(7c) F_{\phi} = 2k^2 \times 0.033 C_n^2(H_0) \int_0^{L/2} n d\eta \int_{-\infty}^{\infty} d\kappa_z \text{sinc}(2\eta\kappa_z) \times$$

$$\left\{ \frac{\left(\frac{H_L}{H_0} - \frac{\eta}{L} \left(\frac{H_L}{H_0} - 1 \right) \right)^{-4/3} \text{sinc} \left(\frac{\kappa_T^2}{k} (L-\eta) \right)}{\left(\left(\frac{1.077}{L_0(H_0) \left(\frac{H_L}{H_0} - \frac{\eta}{L} \left(\frac{H_L}{H_0} - 1 \right) \right)} \right)^2 + \kappa_T^2 + \kappa_z^2 \right)^{11/6}} \right. \\ \left. + \frac{\left(\frac{H_L}{H_0} - \frac{(L-\eta)}{L} \left(\frac{H_L}{H_0} - 1 \right) \right)^{-4/3} \text{sinc} \left(\frac{\kappa_T^2}{k} \eta \right)}{\left(\frac{1.077}{L_0(H_0) \left(\frac{H_L}{H_0} - \frac{(L-\eta)}{L} \left(\frac{H_L}{H_0} - 1 \right) \right)} \right)^2 + \kappa_T^2 + \kappa_z^2)^{11/6}} \right\}$$

Equations (7) can be further simplified after examining the offset in the sinc function in comparison with the width of the term raised to the power 11/6

$$(8) \quad \frac{\kappa_T^2}{2k} = \frac{\lambda}{2L} \quad \kappa_T \ll \kappa_Z$$

Thus the offset of the sinc function is never significant and can be neglected. Equations (7) then reduces to

$$(9a) \quad F_x = 2k^2 \times 0.033 C_n^2(H_0) \int_0^{L/2} r d\eta \int_{-\infty}^{\infty} d\kappa_z \sin(2\eta\kappa_z)$$

$$\times \left\{ \frac{\left(\frac{H_L}{H_0} - \frac{\eta}{L} \left(\frac{H_L}{H_0} - 1 \right) \right)^{-4/3} \left(1 - \cos \left(\frac{\kappa_T^2}{k} (L - \eta) \right) \right)}{\left(\left(\frac{1.077}{L_0(H_0) \left(\frac{H_L}{H_0} - \frac{\eta}{L} \left(\frac{H_L}{H_0} - 1 \right) \right)} \right)^2 + \kappa_T^2 + \kappa_z^2 \right)^{11/6}} + \right.$$

$$\left. + \frac{\left(\frac{H_L}{H_0} - \frac{(L - \eta)}{L} \left(\frac{H_L}{H_0} - 1 \right) \right)^{-4/3} \left(1 - \cos \left(\frac{\kappa_T^2}{k} \eta \right) \right)}{\left(\left(\frac{1.077}{L_0(H_0) \left(\frac{H_L}{H_0} - \frac{(L - \eta)}{L} \left(\frac{H_L}{H_0} - 1 \right) \right)} \right)^2 + \kappa_T^2 + \kappa_z^2 \right)^{11/6}} \right\}$$

$$(9b) F_{\pm} = 2k^2 \times 0.033 C_n^2(H_0) \int_0^{L/2} \eta d\eta \int_{-\infty}^{\infty} d\kappa_z \text{sinc}(2\eta\kappa_z)$$

$$\times \left[\frac{\left(\frac{H_L}{H_0} - \frac{\eta}{L} \left(\frac{H_L}{H_0} - 1 \right) \right)^{-4/3} \left(1 + \cos \left(\frac{\kappa_T^2}{k} (L-\eta) \right) \right)}{\left(\left(\frac{1.077}{L_0(H_0)} \frac{H_L}{H_0} - \frac{\eta}{L} \left(\frac{H_L}{H_0} - 1 \right) \right)^2 + \kappa_T^2 + \kappa_z^2 \right)^{11/6}} \right. \\ \left. \times \frac{\left(\frac{H_L}{H_0} - \frac{(L-\eta)}{L} \left(\frac{H_L}{H_0} - 1 \right) \right)^{-3/2} \left(1 + \cos \frac{\kappa_T^2}{k} \eta \right)}{\left(\left(\frac{1.077}{L_0(H_0)} \frac{H_L}{H_0} - \frac{(L-\eta)}{L} \left(\frac{H_L}{H_0} - 1 \right) \right)^2 + \kappa_T^2 + \kappa_z^2 \right)^{11/6}} \right]$$

$$(9c) F_{\pm} = 2k^2 \times 0.033 C_n^2(H_0) \int_0^{L/2} \eta d\eta \int_{-\infty}^{\infty} d\kappa_z \text{sinc}(2\eta\kappa_z)$$

$$\times \left[\frac{\left(\frac{H_L}{H_0} - \frac{\eta}{L} \left(\frac{H_L}{H_0} - 1 \right) \right)^{-4/3} \sin \left(\frac{\kappa_T^2}{k} (L-\eta) \right)}{\left(\left(\frac{1.077}{L_0(H_0)} \frac{H_L}{H_0} - \frac{\eta}{L} \left(\frac{H_L}{H_0} - 1 \right) \right)^2 + \kappa_T^2 + \kappa_z^2 \right)^{11/6}} \right. \\ \left. + \frac{\left(\frac{H_L}{H_0} - \frac{(L-\eta)}{L} \left(\frac{H_L}{H_0} - 1 \right) \right)^{-4/3}}{\left(\left(\frac{1.077}{L_0(H_0)} \left(\frac{H_L}{H_0} - \frac{(L-\eta)}{L} \left(\frac{H_L}{H_0} - 1 \right) \right) \right)^2 + \kappa_T^2 + \kappa_z^2 \right)^{11/6}} \right]$$

It is useful to have the spectral expressions expressed not in terms of k and C_n^2 , but in terms of the coherence length, r_0 to allow easier comparison with the physical situation.

To do this we consider $F_\phi + F_\phi$, the spectrum of the wave structure function, for the case where the transverse spatial frequency κ_t is larger than $2\pi/L_0$. For this case F_w the wave structure function spectrum reduces to

$$(10a) \quad F_w = 4k^2 \times 0.033 C_n^2(H_0) \int_0^{L/2} \eta d\eta \int_{-\infty}^{\infty} d\kappa_z \frac{\text{sinc}(2\eta\kappa_z)}{(\kappa_T^2 + \kappa_z^2)^{11/6}}$$

$$\times \left\{ \left(\frac{H_L}{H_0} - \frac{\eta}{L} \left(\frac{H_L}{H_0} - 1 \right) \right)^{-4/3} + \left(\frac{H_L}{H_0} - \frac{(L-\eta)}{L} \left(\frac{H_L}{H_0} - 1 \right) \right)^{-4/3} \right\}$$

The width of the sinc function, $\pi/2\eta$, is always less than κ_T , the width of $(\kappa_T^2 + \kappa_z^2)^{-11/6}$ because the size of a typical refractive index fluctuation, $\lambda = 2\pi/\kappa_T$ is always less than the range, η . Thus we have

$$(10b) \quad F_w \approx 2\kappa^2 \times 0.033 C_n^2(H_0) \kappa_T^{-11/3} \int_0^{L/2} d\eta \left[\left(\frac{H_L}{H_0} - \frac{\eta}{L} \left(\frac{H_L}{H_0} - 1 \right) \right)^{-4/3} + \left(\frac{H_L}{H_0} - \frac{(L-\eta)}{L} \left(\frac{H_L}{H_0} - 1 \right) \right)^{-4/3} \right] \\ \times \int_{-\infty}^{\infty} 2\eta d\kappa_z \text{sinc}(2\eta\kappa_z) \\ = 2\pi k^2 \times 0.033 C_n^2(H_0) \kappa_T^{-11/3} (3H_0) \left[1 - \left(\frac{H_0}{H_L} \right)^{1/3} \right]$$

A wave structure function

$$(11a) \quad D_w = 6.88(\rho r_0)^{5/3}$$

corresponds to a spectrum

$$(11b) \quad F_{\omega}(x_T) = \frac{6.88 \Gamma(11/6) 2^{5/3} x^{-11/3}}{r_0^{5/3} 2^2 \times \frac{6}{5} \Gamma(1/6)} = \frac{.245}{r_0^{5/3}} x^{-11/3}$$

Comparing Eqs. (10c) and (11b) we see that

$$r_0 = \left[\frac{6.88 \Gamma(11/6) 2^{5/3}}{(2^2)^2 (6/5) \Gamma(1/6) k^2 \times 0.033 C_n^2(H_0) (3H_0) \left(1 - \left(\frac{H_0}{H_L}\right)^{1/3}\right)} \right]^{3/5}$$

$$= \left[\frac{6.88}{2.91 k^2 (3H_0) C_n^2 \left(1 - \left(\frac{H_0}{H_L}\right)^{1/2}\right)} \right]^{3/5}$$

In Eqs. (9) substitute

$$2k^2 \times 0.033 C_n^2(H_0) = \frac{6.88 (11/6) 2^{5/3}}{2^2 (6/5) (1/6) (3H_0) \left(1 - \left(\frac{H_0}{H_L}\right)^{1/3}\right) r_0^{5/3}}$$

This is included because it is often simpler to work in terms of r_0 rather than k and C_n^2 . Equation (9) and (12) are the results of this writeup. Figures 1 and 3 in the text are the results of computer evaluations of the expressions given.

APPENDIX B

In this appendix we consider the polynomial representation used for the lower frequency portions of the spatial spectrum. Specifically we derive the Karhunen-Loève expansion for a complex function and show that the procedure for diagonalizing the gaussian multivariate distribution is equivalent to solving the Karhunen-Loève problem.

To start we postulate formalism for the Karhunen-Loeve expansion for a random complex function. We apply this to the complex log-amplitude but the development holds for any complex function. Let the random complex function have real and imaginary parts $\ell(\vec{r})$ and $\phi(\vec{r})$ respectively and represent it by the complex function vector

$$(B1) \quad \bar{x}(\vec{r}) = (\ell(\vec{r}) + j\phi(\vec{r}))$$

The covariance functions are represented by a complex function matrix

$$(B2) \quad \bar{C}(\vec{r}', \vec{r}) = \begin{pmatrix} C_{\ell\ell}(\vec{r}', \vec{r}) & -jC_{\ell\phi}(\vec{r}', \vec{r}) \\ jC_{\phi\ell}(\vec{r}', \vec{r}) & C_{\phi\phi}(\vec{r}', \vec{r}) \end{pmatrix}$$

where

$$(B3) \quad C_{\ell\ell}(\vec{r}, \vec{r}) = \langle \ell(\vec{r}') \ell(\vec{r}) \rangle$$

$$(B3b) \quad C_{\ell\phi}(\vec{r}, \vec{r}) = \langle \ell(\vec{r}') \phi(\vec{r}) \rangle$$

$$(B3c) \quad C_{\phi\phi}(\vec{r}, \vec{r}) = \langle \phi(\vec{r}') \phi(\vec{r}) \rangle$$

The spectra of $C_{\ell\ell}(\vec{r}', \vec{r})$, $C_{\ell\phi}(\vec{r}', \vec{r})$ and $C_{\phi\phi}(\vec{r}', \vec{r})$ are calculated in Appendix A for the case of interest. The Karhunen-Loeve integral equation is formally stated

$$(B4) \quad \iint_A d\bar{r} \bar{C}(\bar{r}', \bar{r}) \bar{x}(\bar{r}) = \lambda \bar{x}(\bar{r})$$

where A corresponds to the domain of interest where $\bar{x}(\bar{r})$ and $\bar{\phi}(\bar{r})$ are non-zero. Equation (B4) corresponds to the two coupled integral equations

$$(B5a) \quad \iint_A d\bar{r} C_{\phi\phi}(\bar{r}', \bar{r}) \bar{\phi}(\bar{r}) + \iint_A d\bar{r} C_{\phi x}(\bar{r}', \bar{r}) \bar{x}(\bar{r}) = \lambda \bar{\phi}(\bar{r}')$$

$$(B5b) \quad \iint_A d\bar{r} C_{x\phi}(\bar{r}', \bar{r}) \bar{\phi}(\bar{r}) + \iint_A d\bar{r} C_{xx}(\bar{r}', \bar{r}) \bar{x}(\bar{r}) = \lambda \bar{x}(\bar{r}')$$

Equations (B5) reduce to the standard Karhunen-Loève equations if $\bar{x}(\bar{r})$ and $\bar{\phi}(\bar{r})$ are uncorrelated.

To solve Eqs. (B5) we use a polynomial series representation.

$$(B6a) \quad \bar{x}(\bar{r}) = \sum_{on} \bar{x}_{on} \alpha_n(\bar{r})$$

$$(B6b) \quad \bar{\phi}(\bar{r}) = \sum_{on} \bar{\phi}_{on} \alpha_n(\bar{r})$$

The zero subscripts on the \bar{x}_{on} and $\bar{\phi}_{on}$ are intended to differentiate this expansion from the similar expansion in Eqs. (10) in the main text. The orthonormal set $\{\alpha_n(\bar{r})\}$ should be complete. In practice we will use a truncated series for which the eigenvalues corresponding to the neglected terms are sufficiently small so that the terms dropped are indeed negligible. Inserting solutions (B6) into Eqs. (B5), multiplying through by $\alpha_m(\bar{r}')$ and integrating with respect to \bar{r}' gives

$$(B7a) \quad \sum_1^N C_{\phi\phi, mn} \bar{\phi}_{on} + \sum_1^N C_{\phi x, mn} \bar{x}_{on} = \lambda \bar{\phi}_{om}$$

$$(B7b) \quad \sum_1^N C_{x\phi, mn} \bar{\phi}_{on} + \sum_1^N C_{xx, mn} \bar{x}_{on} = \lambda \bar{x}_{om}$$

where

$$(B7c) \quad C_{\mu\nu mn} = \iiint_{AA'} d\bar{r} d\bar{r}' \alpha_m(\bar{r}') C_{\mu\nu}(\bar{r}', \bar{r}) \alpha_n(\bar{r}) w(\bar{r}) w(\bar{r}') .$$

The subscripts μ and ν in Eq. (B7c) stand for ℓ and ϕ . Equations (B7) can be combined into a single matrix eigenvalue equation,

$$(B8) \quad \bar{C} \bar{y} = \lambda \bar{y}$$

where the matrix \bar{C} contains $C_{\ell\ell}$, $C_{\phi\phi}$ and $C_{\ell\phi}$; and the vector \bar{y} contains both $\bar{\ell}_0$ and $\bar{\phi}_0$ as indicated in Eqs. (B9)

$$(B9a) \quad \bar{C} = \begin{pmatrix} C_{\ell\ell 11} & & & C_{\phi\phi 11} \\ & C_{\ell\ell \mu\nu} & & C_{\phi\phi \mu\nu} \\ C_{\ell\phi 11} & & C_{\phi\ell 11} & \\ & C_{\ell\phi \mu\nu} & & C_{\phi\ell \mu\nu} \end{pmatrix}$$

$$(B9b) \quad \bar{y} = (\ell_{01}, \ell_{02}, \dots, \ell_{0N}, \phi_{01}, \phi_{02}, \dots, \phi_{0N})$$

Equation (B8) is simply solved by the well-known procedure which starts with setting the determinant

$$(B10) \quad |\bar{C} - \lambda \bar{I}| = 0$$

The resultant values for the eigenvalues, λ_p then give the eigenvectors \bar{y}_p and the diagonalizing matrix \bar{M}_0 whose columns are the normalized eigenvectors. The diagonalizing transformation is

$$(B11) \quad \bar{y} = \bar{M}_0 \bar{z}$$

We now display the connection with the multivariate distribution indicated in the text. Multiplying Eq. (B8) from the left by $\lambda^{-1} C^{-1}$ gives

$$(B12a) \quad \bar{Q} \bar{y} = \lambda^{-1} \bar{y}$$

where

$$(B12b) \quad \bar{Q} = \bar{C}^{-1}$$

Equations (B12) are identical with Eq. (15) in the text if we equate the orthonormal polynomials $\psi_n(r)$ and $\alpha_n(r)$. Further the eigenvalues of the \bar{Q} matrix in the multivariate distribution are merely the reciprocals of those of the Karhunen-Loève problem and the eigenvectors y_n and w_n are identical.

This completes the desired demonstrations: the derivation of the associated Karhunen-Loève problem and the demonstration of the equivalence of the multivariate and Karhunen-Loève approaches.

APPENDIX C

We now derive expressions for the functions $U_n(K_{x0}, L_{x0})$ and $V(M_{x0}, N_{x0})$ which were introduced in the main text Eqs. (29) in the main text.

Without loss of generality, we display only the development for the phase. To begin, assume that the orthonormal functions are polynomials in x and y so that in general

$$(C-1) \quad \psi_n(x, y) = \sum_p \sum_q g_{npq} x^p y^q.$$

Then for a square aperture the function $V_n(M_{x0}, N_{x0})$ can be written in the form

$$(C-2) \quad V_n(M_{x0}, N_{x0}) = \sum g_{npq} I_p(M) I_q(N)$$

where

$$(C-3) \quad I_q(N) = \int_{-x_0/2}^{x_0/2} dx x^q \operatorname{sinc} \pi \left[\frac{x}{x_0} - (N-33) \right].$$

The function $U(K_{x0}, L_{x0})$ in Eq. (29a) can also be written in the more detailed form,

$$(C-4) \quad U(K_{x0}, L_{x0}) = \sum_p \sum_q g_{npq} T_p(K_{x0}) T_q(L_{x0})$$

where

$$(C-5) \quad T_i(K_{x0}) = \kappa_0^2 \sum_{M=1}^N I_i(M_{x0}) e^{\frac{i2\pi}{N}(M-1)(K-1)}.$$

For the polynomials listed in Eqs. (31) the functions $U_0(K_{x0}, L_{x0})$ through $U_9(K_{x0}, L_{x0})$ have the following form:

$$(C6a) \quad U_0(Kk_0, Lk_0) = T_0(K_{\nu_0})T_0(L_{\nu_0})$$

$$(C6b) \quad U_1(Kk_0, Kk_0) = 2\sqrt{3} T_0(K_{\nu_0})T_1(L_{\nu_0})$$

$$(C6c) \quad U_2(Kk_0, Lk_0) = -2\sqrt{3}T_1(K_{\nu_0})T_0(L_{\nu_0})$$

$$(C6d) \quad U_3(Kk_0, Lk_0) = 6\sqrt{\frac{5}{2}} [T_0(K_{\nu_0})T_2(L_{\nu_0}) + T_2(K_{\nu_0})T_0(L_{\nu_0}) \\ - \frac{1}{6} T_0(K_{\nu_0})T_0(L_{\nu_0})]$$

$$(C6e) \quad U_4(Kk_0, Lk_0) = 6\sqrt{\frac{5}{2}} [T_0(K_{\nu_0})T_2(K_{\nu_0}) - T_2(K_{\nu_0})T_0(L_{\nu_0})]$$

$$(C6f) \quad U_5(Kk_0, Lk_0) = -12 T_1(K_{\nu_0})T_1(L_{\nu_0})$$

$$(C6g) \quad U_6(Kk_0, Lk_0) = 12\sqrt{15} [T_2(K_{\nu_0})T_1(2K_{\nu_0}) - \frac{1}{12} T_0(K_{\nu_0})T_1(L_{\nu_0})]$$

$$(C6h) \quad U_7(Kk_0, Lk_0) = -12\sqrt{15}[T_1(K_{\nu_0})T_2(L_{\nu_0}) - \frac{1}{12} T_1(K_{\nu_0}) T_0(L_{\nu_0})]$$

$$(C6i) \quad U_8(Kk_0, Lk_0) = 20\sqrt{7} [T_0(K_{\nu_0})T_3(L_{\nu_0}) - \frac{3}{20} T_0(K_{\nu_0})T_1(L_{\nu_0})]$$

$$(C6j) \quad U_9(Kk_0, Lk_0) = -20\sqrt{7} [T_3(K_{\nu_0})T_0(L_{\nu_0}) - \frac{3}{20} T_1(K_{\nu_0})T_0(L_{\nu_0})]$$

APPENDIX D

This appendix contains a listing of the sixty four eigenvalues of a solution for the Karhunen-Loeve integral equation assuming an eight by eight grid for the aperture plane. The correlation function corresponded to the phase function calculated in Appendix A.

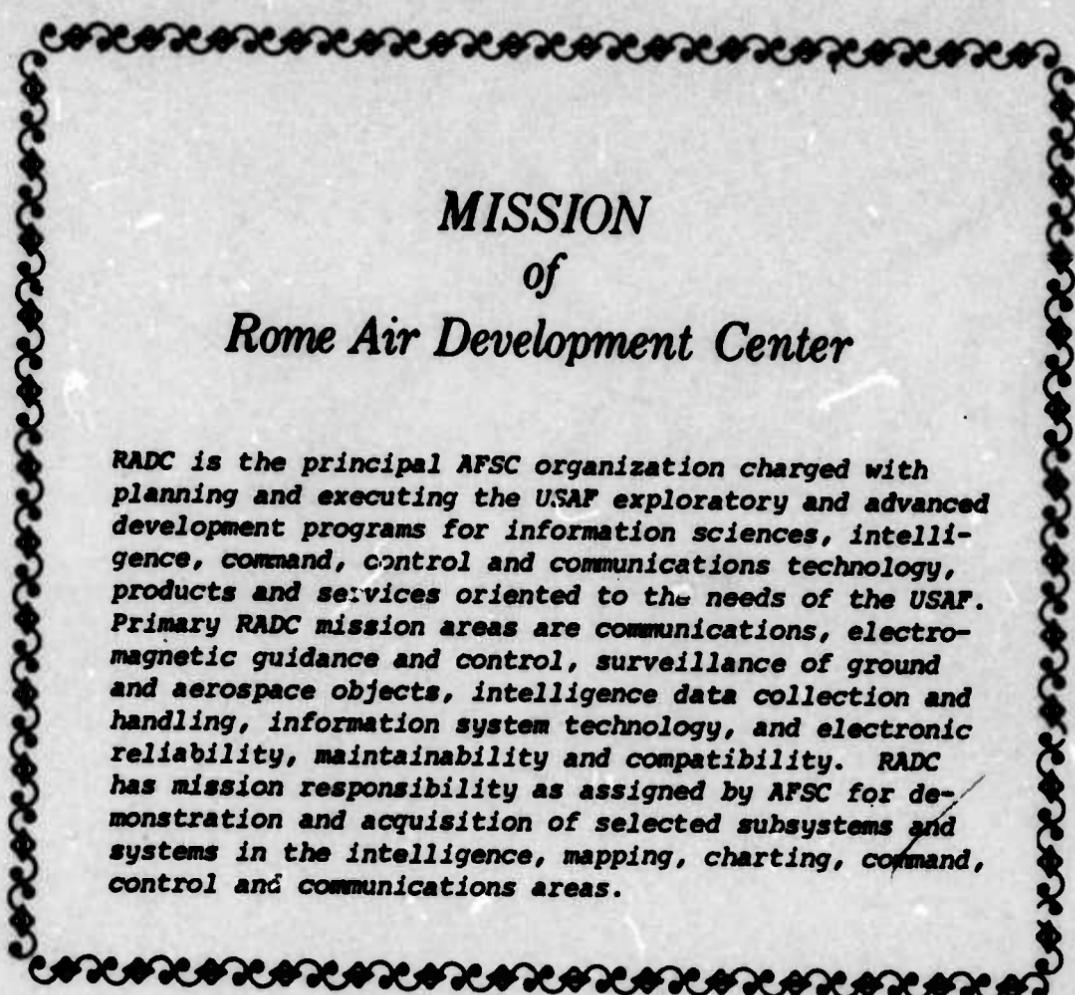
EIGENVALUES

.9999E 0 -(0,0)	.1875E -5 -(0,1)	.1875E -5 -(1,0)	.1599E -6 -(1,1)	.1347E -6 (0,2)
.9220E -7 -(2,0)	.4423E -7 -(2,1)	.4423E -7 -(1,2)	.2537E -7 -(0,3)	.2537E -7 (3,0)
.1802E -7	.1590E -7	.1323E -7	.8994E -8	.8636E -8
.8486E -8	.8486E -8	.6235E -8	.6234E -8	.4873E -8
.4575E -8	.4162E -8	.4044E -8	.4043E -8	.3321E -8
.3201E -8	.3015E -8	.3014E -8	.2565E -8	.2565E -8
.2281E -8	.2254E -8	.2109E -8	.2034E -8	.2006E -8
.2005E -8	.1958E -8	.1742E -8	.1712E -8	.1586E -8
.1586E -8	.1563E -8	.1563E -8	.1479E -8	.1474E -8
.1461E -8	.1461E -8	.1344E -8	.1343E -8	.1264E -8
.1249E -8	.1232E -8	.1203E -8	.1199E -8	.1072E -8
.1071E -8	.1065E -8	.1065E -8	.9599E -9	.9580E -9
.9478E -9	.8773E -9	.8772E -9	.8269E -9	

REFERENCES

- [Bradley, Lee, 1974] Private Communication.
- [Brown, W.P., 1974], Topical Meeting on Propagation Through Turbulence, University of Colorado, Boulder, Colorado, July 9, 11, 1974.
- [Davenport, W.B., Jr. and W.L. Root, 1958], An Introduction to the Theory of Random Signals and Noise, McGraw Hill Book Co.
- [Fried, D.L., 1965] Statistics of Wavefront Distortion, Jour. Opt. Soc. Am 55, 1472.
- [Hogge, C.B., 1973] Private Communication.
- [Hogge, 1974] It is not necessary to generate the array in position space and transform it. The generated random array has all the properties necessary for use directly in the frequency plane. See Davenport (1958) p. 168, problem 7.
- [McGlamery, B.J. 1974] Compensated Imaging Program Review Meeting, Naval Post Graduate School, Monterey, California, November 5.
- [Noll, R.S. 1974] Compensated Imaging Program Review Meeting, Naval Postgraduate School, Monterey, California, November 5.
- [Tatarski, V.I. 1971] The Effects of the Turbulent Atmosphere on Wave Propagation, Reprint TT 68-50464, U.S. Dept of Commerce, N.T.I.S., Springfield, Va. 22151.

U.S. GOVERNMENT PRINTING OFFICE: 1975-614-357/2



MISSION
of
Rome Air Development Center

RADC is the principal AFSC organization charged with planning and executing the USAF exploratory and advanced development programs for information sciences, intelligence, command, control and communications technology, products and services oriented to the needs of the USAF. Primary RADC mission areas are communications, electromagnetic guidance and control, surveillance of ground and aerospace objects, intelligence data collection and handling, information system technology, and electronic reliability, maintainability and compatibility. RADC has mission responsibility as assigned by AFSC for demonstration and acquisition of selected subsystems and systems in the intelligence, mapping, charting, command, control and communications areas.